Master's thesis

NTNU
Norwegian University of Science and Technology
Faculty of Engineering
Department of Marine Technology

Elias Gauslaa

Navigation, guidance, and control for autonomous docking of ships

Master's thesis in Marine Technology
Supervisor: Roger Skjetne
June 2020

NTNU
Norwegian University of
Science and Technology

Elias Gauslaa

Navigation, guidance, and control for autonomous docking of ships

Master's thesis in Marine Technology
Supervisor: Roger Skjetne
June 2020

Norwegian University of Science and Technology
Faculty of Engineering
Department of Marine Technology

NTNU
Norwegian University of
Science and Technology

NTNU Trondheim
Norwegian University of Science and Technology
Department of Marine Technology

MASTER OF TECHNOLOGY THESIS DEFINITION (30 SP)

Name of the candidate: Gauslaa, Elias

Field of study: Marine control engineering

Thesis title (Norwegian): Navigasjon, gaiding og styring for autonomy kailegging av skip

Thesis title (English): Navigation, guidance, and control for autonomous docking of ships

Background
For ships, the ability to safely perform docking and takeoff maneuvers are especially critical and involve complex maneuvering by a skilled ship pilot. This involves understanding of:

- the ship dynamics (inertial delays, responses to currents, wind gusts, and propulsion, etc.),
- the hydrodynamic effects of maneuvering near harbor structures,
- the optimal entrance paths and speed regulation for safe docking,
- the sensors, displays, and monitoring variables to use for necessary information feedback, and
- communication between the different crew members involved in the maneuver.

The objective of this thesis is to develop an autonomous docking controller (ADC) enabling autonomous autodocking of ships, utilizing a conventional sensor suite combined by proximity sensors along the ship side. Solutions to enable simple situational reactiveness using the proximity sensors should also be explored. The thesis will consider fully actuated ships, and navigation, guidance, and control systems most be designed and put together to form the autonomous docking controller. The proximity sensors should be used with the path-generator and path-following system, such that a conventional motion controller and observer can be used.

Work description
1. Perform a background and literature review to provide information and relevant references on:
   - Ship maneuvering and docking practices.
   - Relevant ship sensors and instrumentation.
   - Relevant navigation filter designs.
   - Methods for generating a path from waypoints.
   - Relevant motion guidance and control designs.

   Write a list with abbreviations and definitions of terms and symbols, relevant to the literature study and project report.
2. Formulate the control problem for autodocking a ship, including definition of a case study, description of setup, vessel and its equipment, dynamical models, operation workspace, actuation, and specific assumptions and delimitations. Conclude with a problem statement
3. Investigate and develop a path-planning algorithm for autonomous docking, that takes the ship from a harbor maneuvering mode and prepares it for docking.
4. Study, conclude, and implement a path-generating algorithm for docking of the ship. Discuss what and how the sensor measurements could be used to generate the path and to perform the path-following during the operation.
5. Design and implement a control function enabling path-following and autonomous docking, by combining the conventional navigation sensors with proximity sensors. Explore ways to extend the ADC with situational reactiveness based on the proximity sensor measurements.
6. Develop an observer capable of noise filtering and dead reckoning, according to your case study.
7. Prepare CSEI for use in experiments with installation of proximity sensors (and also as a simulation model if lab becomes unavailable). Tune the VSP servos, measure actuator forces, and verify input

to thruster mapping and update the handbook with methods and results. Calibrate the simulation model according to physical testing. Implement the ADC mode for CSEI.

8. Test your ADC on CSEI in MC-lab as a proof of concept, or as a simulation study if lab becomes unavailable. Present the experimental and/or simulation setup. Analyze and discuss the results.

Specifications

Every weekend throughout the project period, the candidate shall send a status email to the supervisor and co-advisors, providing two brief bulleted lists: 1) work done recent week, and 2) work planned to be done next week.

The scope of work may prove to be larger than initially anticipated. By the approval from the supervisor, described topics may be deleted or reduced in extent without consequences with regard to grading.

The candidate shall present personal contribution to the resolution of problems within the scope of work. Theories and conclusions should be based on mathematical derivations and logic reasoning identifying the various steps in the deduction.

The report shall be organized in a logical structure to give a clear exposition of background, problem, design, results, and critical assessments. The text should be brief and to the point, with a clear language. Rigorous mathematical deductions and illustrating figures are preferred over lengthy textual descriptions. The report shall have font size 11 pts., and it is not expected to be longer than 70 A4-pages, 100 B5-pages, from introduction to conclusion, unless otherwise agreed upon. It shall be written in English (preferably US) and contain the elements: Title page, abstract, acknowledgement, project definition, list of symbols and acronyms, table of contents, introduction (project motivation, objectives, scope and delimitations), background/literature review, problem formulation, method, results, conclusions with recommendations for further work, references, and optional appendices. Figures, tables, and equations shall be numerated. The original contribution of the candidate and material taken from other sources shall be clearly identified. Work from other sources shall be properly acknowledged using quotations and a Harvard citation style (e.g. *natbib* Latex package). The work is expected to be conducted in an honest and ethical manner, without any sort of plagiarism and misconduct, which is taken very seriously by the university and cause consequences. NTNU can use the results freely in research and teaching by proper referencing, unless otherwise agreed upon.

The thesis shall be submitted with an electronic copy to the main supervisor and department according to NTNU administrative procedures. The final revised version of this thesis description shall be included after the title page. Computer code, pictures, videos, dataseries, etc., shall be included electronically with the report.

Start date: 15th of January 2020 **Due date:** 10th of June, 2020

Supervisor: Roger Skjetne
Co-advisor(s): Zhengru Ren, Mathias Marley, Einar Ueland (MC-Lab issues only)

Trondheim, 24.03.2020

Roger Skjetne

Digitally signed by Roger Skjetne
Date: 2020.03.24 12:03:53 +01'00'

Roger Skjetne
Supervisor

Abstract

This thesis presents an autonomous docking controller utilizing a traditional sensor suite aided by proximity sensors. The docking controller is able to autonomously dock a marine surface vessel in a safe and controlled manner, and some basic situational awareness and reactiveness are implemented.

Development of the autonomous docking controller is divided into three main components, the navigation, guidance, and control systems. The guidance system consists of a path planner which decides where to place the waypoints of the operation, and a path generator which generates a trajectory for the vessel to follow using a hybrid path parametrization to smoothly and continuously concatenate the waypoints. The navigation system employs a nonlinear passive observer to filter measurements and to generate signals for unmeasured states, needed in the control system. An uncoupled cascaded backstepping controller is used in the control system to maneuver the vessel according to the desired trajectory and desired heading.

The autonomous docking operation is divided into two phases. The first one consists of navigating the vessel to a point outside the designated docking location, while the second phase consists of moving the vessel slowly towards the dock and stopping a desired distance from the quayside. The chosen guidance laws generate a docking path, and manipulate the speed of the vessel during the operation, making it come to rest at the end of each phase. The proximity sensors are used to provide a heading correction for the desired heading when the ship arrives at the end of the first phase, as well as manipulating the speed assignment during the second phase based on the distance to the quay. Solutions to enable situational awareness based on the proximity sensors measurements are explored, as well as two reactions to an eventual detected danger.

Both normal operation with different initial positions with respect to the dock, and operations testing the situational awareness and reactiveness are tested in simulations. For simulations, the C/S Enterprise was modeled, and values found in experiments was used for the thruster modeling. The simulations show good performance of the autonomous docking controller.

Sammendrag

Denne oppgaven presenterer en autonom dokkingkontroller som bruker tradisjonelle sensorer, med hjelp av nærhetssensorer. Dokkingkontrolleren er i stand til å legge et marint overflatefartøy til kai autonomt på en sikker og kontrollert måte, og enkel situasjonsbevissthet og reaktivitet blir implementert.

Utvikling av den autonome dokkingkontrolleren er delt inn i tre hovedkomponenter, navigasjons-, gaidings- og kontrollsystemet. Gaidingssystemet består av en baneplanlegger som bestemmer hvor man skal plassere veipunktene for operasjonen, og en banegenerator som genererer en bane for fartøyet å følge, ved å bruke hybrid baneparametrisering for å kontinuerlig koble sammen veipunktene. Navigasjonssystemet benytter en ikke-lineær passiv estimator til å filtrere målinger og for å generere signaler for umålte tilstander brukt av kontrollsystemet. En dekoblet kaskadert tilbakestegskontroller brukes i kontrollsystemet for å manøvrere fartøyet i henhold til ønsket bane og orientering.

Den autonome dokkingoperasjonen kan deles inn i to faser. Den første består i å navigere fartøyet til et punkt utenfor det angitte kaiplassen, mens den andre fasen består i å bevege fartøyet sakte mot kaien og stoppe en ønsket avstand fra kaikanten. De valgte gaidingslovene genererer en dokkingbane, og manipulerer fartøyets fart under operasjonen slik at det stanser på slutten av hver fase. Nærhetssensorene brukes til å gi en retningskorreksjon for ønsket kurs når skipet ankommer slutten av den første fasen, samt manipulere hastigheten i den andre fasen basert på avstanden til kai. Løsninger for å muliggjøre situasjonsbevissthet basert på målingene fra nærhetssensorene blir utforsket, samt to reaksjoner på eventuelt oppdaget fare.

Både normal drift med forskjellige utgangsposisjoner med hensyn til kaien, og testing av situasjonsbevissthet og reaktivitet testes i simuleringer. For simuleringene ble C/S Enterprise modellert, og verdier funnet i eksperimenter ble brukt til aktuatormodellering. Simuleringene viser god ytelse av den autonome dokkingkontrolleren.

Preface

This master's thesis is the culmination of my studies of Marine Technology at the Norwegian University of Science and Technology. I have spent the last five years learning and developing not only my professional knowledge, but also getting to know myself as a person. This thesis was written in the spring of 2020, a semester that has been very much different than the others I have experienced during my years as a student. As the global pandemic COVID-19 led to a lockdown of a great part of the community, society and peoples everyday life, a significant deal of this thesis has been written without access to the university facilities. Due to this, the thesis work has been mostly independent work, but I have received assistance via e-mail and my supervisor, Roger Skjetne, and co-advisors have been available for online meetings.

This thesis is in some extent a continuation of the project thesis from the fall of 2019, and the thesis work started off in early January with a couple of weeks in the laboratory to work on the model ship C/S Enterprise. Einar Ueland and Torgeir Wahl were good assets in this process. However, due to COVID-19 the laboratory experiments was removed from this thesis, and a simulation study was chosen as replacement. The work done in the lab by my fellow students and I are still valuable for the department, and later courses and students. Writing of the thesis started shortly after the lab work, finishing the problem formulation, background and literature review, and modeling, before starting to actually code and develop the autonomous docking controller. Writing of the thesis and developing of code has been done in tandem, evenly spreading out the work on each part over the semester. Before the school lockdown, there were common guidance meetings with Roger Skjetne, as well as individual guidance meetings every other week with co-advisor Zhengru Ren. After lockdown, Ren has been available for online guidance as a continuation of the biweekly meetings, and was a good asset in the early stages of writing. Skjetne has provided me with notes and documents, guiding and helping me throughout the process of development and implementation. Also, both Skjetne and co-advisors have at all times been available to ask for guidance and have quickly responded to my mails, even though the lockdown has led to a mindset of independence.

Elias Gauslaa
June 8, 2020, Trondheim.

Acknowledgments

My supervisor, Professor Roger Skjetne, has been of great importance in regards to supervision, guidance and support during my work with this thesis. His advice and understanding of the subject has been of great help for me in the process of solving the problems encountered, and he has provided me with important references, notes and ideas. Thank you.

I would like to thank my co-advisor Zhengru Ren for good help, feedback, and advice during my work. Zhengru has shown great dedication and interest in me and my work. I would also like to thank Einar Ueland and Mathias Marley for help regarding laboratory work and work with the model ship C/S Enterprise. Torgeir Wahl has also been a valuable asset when it comes to technical challenges and issues in the laboratory.

The institution NTNU, and the Department of Marine Technology should also be thanked for facilitating continued work and progression after the lockdown, which was introduced as a response to the COVID-19 outbreak.

Last, but not least, I would like to thank my fellow student Jakob Stensvik Jensen. He has been an important source of support and feedback, as well as a great sparring partner.

Contents

1 Introduction **1**

1.1 Motivation . . . 1
1.2 Objectives . . . 2
1.3 Scope . . . 2
1.4 Thesis contribution . . . 2
1.5 Outline of thesis . . . 3

2 Background **5**

2.1 Ship maneuvering and docking . . . 5
2.1.1 The golden rules of berthing . . . 5
2.1.2 Accidents related to docking . . . 5
2.1.3 Ship factors affecting handling and maneuvering . . . 6
2.1.4 Berthing under environmental influences . . . 7
2.1.5 Hydrodynamic effects . . . 7
2.1.6 Common docking procedures . . . 8
2.1.7 Docking speed . . . 9
2.2 Relevant ship sensors and instrumentation . . . 10
2.3 Relevant navigation filter designs . . . 12
2.3.1 Lowpass, highpass and bandpass filters . . . 12
2.3.2 Kalman filter . . . 12
2.3.3 Nonlinear passive observer . . . 13
2.4 Path generation . . . 14
2.5 The maneuvering problem and maneuvering control designs . . . 15
2.5.1 PID controller . . . 15
2.5.2 Backstepping controller . . . 15

3 Problem formulation **17**

3.1 System description . . . 17
3.2 Modeling . . . 19
3.2.1 Reference frames . . . 19
3.2.2 Simulation model . . . 19

3.2.3 Control design model . . . 20
3.3 Problem statement . . . 22
3.3.1 System overview . . . 22
3.3.2 Navigation system . . . 22
3.3.3 Guidance system . . . 23
3.3.4 Control system . . . 24

4 Proximity sensor modeling **25**

5 Navigation system **27**
5.1 Nonlinear passive observer . . . 27

6 Guidance system **29**
6.1 Path planning . . . 29
6.2 Path generation . . . 32
6.2.1 A $\mathcal{C}^r$ path generated from waypoints . . . 32
6.2.2 Hybrid parametrization of a $\mathcal{C}^r$ path . . . 33
6.3 Guidance laws . . . 34
6.3.1 Phase 1 . . . 34
6.3.2 Phase 2 . . . 36
6.3.3 Combined guidance system . . . 38
6.3.4 Situational reactiveness based on proximity sensor measurements . . . 38

7 Control system **43**
7.1 Motion controller . . . 43
7.2 Control allocation . . . 48

8 Simulation setup **49**
8.1 CyberShip Enterprise I . . . 49
8.2 Preparatory work on CSEI . . . 50
8.3 Implementation of thruster allocation and dynamics of CSEI . . . 51

9 Results **53**
9.1 Simulations . . . 53
9.2 Autonomous docking . . . 55
9.2.1 Regular operation . . . 56
9.2.2 Regular operation: Near-parallel entry path . . . 58
9.2.3 Regular operation: Sharp entry path . . . 60
9.2.4 Situational reactiveness: Obstacle entering docking path . . . 62
9.3 Discussion . . . 66

10 Conclusions and further work **69**

10.1 Conclusions 69
10.2 Further work 70

Bibliography **71**

A Removing second to last WP **73**

B Animations of simulations **75**

List of Figures

2.1 Docking procedures [Courtesy of Murdoch et al. (2012)]. 9
2.2 Examples of both Dubins and cubic spline interpolation [Courtesy of Fossen (2011)]. 14

3.1 Docking operation overview. 18
3.2 ADC components. Adapted from Fossen (2011). 22

4.1 Explanatory figure for proximity sensor modeling. 25

6.1 Different path planning algorithms, with increasing number of waypoints and tighter constraint on the perpendicularity of the normal vector and the dock. 30
6.2 Path planning with same inital position but with different dock offset angles. 32
6.3 Path generation with different lambda values. 34
6.4 Plot of $\tanh\left(\frac{x}{0.5}\right)$. 36
6.5 Docking operation and sensor measurements. 37
6.6 Illustration of obstacle entering the field of view of proximity sensor 2. . . . 39
6.7 d_2 measurement as a function of time. The vessel is moving towards the dock with a constant speed. An obstacle enters the field of view at 50 seconds, and remains there for the rest of the simulation. The ship continues towards the dock, and collides with the obstacle at 70 seconds. 40
6.8 Flowchart of a situational reactiveness system. 41

8.1 Technical drawing of CSEI 50

9.1 Measured position and heading compared to observer estimates. 54
9.2 Estimated velocities and bias. 54
9.3 Position and heading. 56
9.4 Measured and desired position and heading, and true and estimated velocities. 56
9.5 Desired and yielded forces, and proximity sensor measurements. 57
9.6 Position and heading. 58
9.7 Measured and desired position and heading, and true and estimated velocities. 58
9.8 Desired and yielded forces, and proximity sensor measurements. 59

9.9 Position and heading. 60
9.10 Measured and desired position and heading, and true and estimated velocities. 60
9.11 Yielded and desired forces, and proximity sensor measurements. 61
9.12 Position and heading during the operation. 62
9.13 Measured and desired position and heading, and true and estimated velocities. 63
9.14 Yielded and desired forces, and proximity sensor measurements. 63
9.15 Position and heading during operation. 64
9.16 Measured and desired position and heading, and true and estimated velocities. 65
9.17 Desired and yielded forces and moment, and proximity sensor measurements. 65

A.1 Position and heading. 73
A.2 Measured and desired position and heading, and true and estimated velocities. 74
A.3 Yielded and desired forces, and proximity sensor measurements. 74

B.1 QR-codes to animations. 75
B.2 QR-codes to animations. 76
B.3 QR-codes to animations. 76

List of Tables

6.1 Constants and coefficients 31

8.1 CSEI main data 49
8.2 Actuator positions of CSEI 50
8.3 CSEI rigid body, added mass and damping coefficients. Courtesy of NTNU (2020). 50

9.1 ADC simulation parameters. 53
9.2 Locations of proximity sensors in body frame. 55

Abbreviations and symbols

ADC	Autonomous docking controller
ADCP	Acoustic Doppler current profiler
ASV	Autonomous surface vehicle
BT	Bow thruster
CDGPS	Carrier Differential GPS
CLF	Control Lyapunov function
CSEI	CyberShip Enterprise I
DGPS	Differential GPS
DOF	Degree of freedom
DP	Dynamic positioning
DVL	Doppler velocity log
EKF	Extended Kalman filter
GNSS	Global navigation satellite system
GPS	Global positioning system
HIL	Hardware-in-the-loop
HPR	Hydroacoustic position reference
IMU	Inertial measurement unit
INS	Inertial navigation system
KF	Kalman filter
MC-lab	Marine cybernetics laboratory
NED	North-east-down frame
NPO	Nonlinear passive observer
PID	Proportional–integral–derivative
RB	Rigid body
RTK GPD	Real-time kinematic GPS
SOG	Speed over ground
ULCV	Ultra large container vessel
VSP	Voith Schneider propeller
WP	Waypoint

$\boldsymbol{\alpha}$	Virtual control matrix
$\boldsymbol{\alpha_p}$	Virtual control matrix for position
α_ψ	Virtual control for heading
α_i	Commanded azimuth angle for actuator i
Δ_d	Difference in proximity sensor measurements
$\bar{\Delta}_d$	Moving average of difference in proximity sensor measurements
Δ_l	Difference in body-frame x position of proximity sensor 1 and 2
Δ_u	tanh-gain for υ_{s_1}
Δ_{s2}	tanh-gain for u_{dock} if danger is detected
Δ_p	tanh-gain for υ_{s_2}
Δ_x	Distance from second to last waypoint to initial position along x-axis
Δ_y	Distance from second to last waypoint to initial position along y-axis
δ_ψ	Activation function for heading correction
δ_{dock}	Activation function for Phase 2
ϵ_ψ	Accepted heading error before initiating Phase 2
ϵ_1, ϵ_2	Threshold for detected drop to be considered a danger
$\boldsymbol{\eta}$	Vessel position and heading
$\hat{\boldsymbol{\eta}}$	Estimated vessel position and heading
$\boldsymbol{\eta_0}$	Initial vessel position and heading
$\boldsymbol{\eta_d}$	Desired position and heading
$\boldsymbol{\eta_{dock}}$	Dock position and orientation
$\boldsymbol{\eta_m}$	Measured position and heading
$\boldsymbol{\eta_w}$	First order wave induced motion
$\boldsymbol{\nu}$	Vessel speed and heading rate
$\hat{\boldsymbol{\nu}}$	Estimated vessel speed and heading rate
$\boldsymbol{\nu_c}$	Current velocity vector
$\boldsymbol{\nu_r}$	Relative speed and heading rate
$\boldsymbol{\upsilon}$	Speed assignment vector
υ_s	Speed assignment
υ_{s_1}, υ_{s_2}	Speed assignment for s_1 and s_2
$\boldsymbol{\tau}$	Control forces and moment
$\boldsymbol{\tau_d}$	Desired forces and moment
τ_x, τ_y, τ_n	Thrust and moment in surge, sway, and yaw
ψ	Heading
ψ_ω	Measurement noise in heading measurements
ψ_{corr}	Heading correction
ψ_d	Desired heading
ψ_{d_1}	Desired heading during Phase 1
ϕ_{dock}	Orientation of dock
ρ_1, ρ_2	Tuning functions

λ	Hybrid path design parameter
μ_1, μ_2	Non-negative tuning constants
$\boldsymbol{\omega}$	Maneuvering update law matrix
ω_1, ω_2	Maneuvering update laws
ω_{ci}, ω_{0i}	Filter cut-off and wave peak frequency
$a_{i,j}$, $b_{i,j}$	Hybrid path parameter coefficients
$\mathbf{B}$	Extended thrust configuration matrix
B	Beam
$\mathbf{b}$	Bias
$\hat{\mathbf{b}}$	Estimated bias
$\mathcal{C}^r$	Continuous path of differentiability r
$\mathbf{C}$	Coriolis-centripetal matrix
$c_{1,x}$, $c_{1,y}$	Distance coefficient in x and y for p_1
$c_{2,x}$, $c_{2,y}$	Distance coefficient in x for p_2
$\mathbf{D}$	Damping matrix
d	Distance chosen to be compared to d_{ref}
$\tilde{d}$	Difference between d and d_{ref}
d_1	Measurement from proximity sensor 1
d_2	Measurement from proximity sensor 2
d_i	Modeled distance from proximity sensor i to dock
d_{ph1}	Distance out from the dock the last waypoint is placed
d_{ref}	Desired distance between ship and dock
d_{tang}	Distance second to last waypoint is placed behind the last waypoint
$\mathbf{f}$	Thrust matrix
$f_{cmd,i}$	Commanded thrust for thruster i
$f_{i,x}$, $f_{i,y}$	Desired thrust in body-fixed x- and y-direction from thruster i
f_{s_i}	Line normal from the ship side from proximity sensor
f_{dock}	Line representing the dock
f_{max}	Max available thrust
$\mathbf{I}$	Identity matrix
I_z	Moment of inertia about z-axis
$\mathbf{K_1}, \mathbf{K_2}, \mathbf{K_3}, \mathbf{K_4}$	Gain matrices, used both in observer and controller
$\mathbf{K_{1,p}}$	Gain matrix for position in motion controller
$k_{1,\psi}$	Gain for heading in motion controller
k_i	Scale of thrust for thruster i
L	Length of vessel
L_{oa}	Length of model ship
$L_{x,BT}$	x length to BT
$L_{x,VSP}$, $L_{y,VSP}$	x and y length to VSP
l_1, l_2	x length to proximity sensor 1 and 2 in body-frame
$\mathbf{M}$	Vessel inertia matrix

m	Mass of model ship
$\mathbf{M_{RB}}$	Rigid body mass
$\mathbf{M_A}$	Added mass
N	Number of path segments / moment in yaw
$\mathbf{N_d}$	Normal vector
$\mathbf{N_s}$	Normal vector to the line between proximity sensors
n	Number of waypoints
p	Position of ship in global frame
p_0	Initial position of ship in global frame
$\mathbf{p_d}$	Desired path
$\mathbf{p_{d_1}}$	Desired path in Phase 1
$\mathbf{p_{dock}}$	Desired path in Phase 2
p_{dock}	Position of dock in global frame
p_n	Target position outside dock
p_{s_i}	Position of proximity sensor in global frame
$p^b_{s_i}$	Position of proximity sensor i in body frame.
p_{int}	Intersection point of lines f_{s_i} and f_{dock}
$\mathbf{R}(\psi)$	Rotation matrix
r	Body fixed yaw rate
$\mathbf{S}$	Skew-symmetric matrix
$\mathbf{S_2}$	Skew-symmetric matrix
$\mathbf{s}$	Vector containing s_1 and s_2
s_1	Tangential path variable
s_2	Normal path variable
$\mathbf{T_1}$, $\mathbf{T_2}$	Time constant matrices for subsystems $\mathbf{z_1}$ and $\mathbf{z_2}$
$\mathbf{T_{1,p}}$	Time constant matrix for position
$T_{1,\psi}$	Time constant for heading
$\mathbf{T_d}$	Tangential vector
T_u, T_v, T_r	Time constants for $\mathbf{z_2}$-subsystem
T_x, T_y, T_ψ	Time constants for $\mathbf{z_1}$-subsystem
t	Time
$\mathbf{u}$	Control input vector
u	Body-fixed velocity in surge
u_d	Desired speed in s_1-direction
u_{dock}	Desired speed in s_2-direction
u_i	Control input to thruster i
v	Body-fixed velocity in sway
$\mathbf{V_{1,p}}$	Step 1 Lyapunov function for position
$V_{1,\psi}$	Step 1 Lyapunov function for heading
$\mathbf{V_2}$	Step 2 Lyapunov function

v, w	Zero mean Gaussian white and process noise
$\mathcal{WP}$	Set of waypoints
X, Y, N	Forces and moment in surge, sway, and yaw
X_d, Y_d, N_d	Desired forces and moment in surge, sway, and yaw
$X_u, Y_{v/r}, N_{v/r}$	Hydrodynamic damping coefficients
$X_{\dot{u}}, Y_{\dot{v}}, Y_{\dot{r}}, N_{\dot{r}}$	Hydrodynamic added mass coefficients
x, y, z	Position
x_0, y_0, z_0	Initial position of vessel
x_d, y_d, ψ_d	Desired position and heading overall
x_{d_1}, y_{d_1}	Desired path tangential position Phase 1
x_g, y_g	Position of center of gravity
$x^b_{s_i}$, $y^b_{s_i}$	x- and y-position of proximity sensor i in body-frame
$\mathbf{y_3}$	Heading measurement
$\tilde{\mathbf{y}}$	Estimation error
$\mathbf{z_1}$	Error state matrix
$\mathbf{z_{1,p}}$	Position error state variable
$z_{1,\psi}$	Heading error state variable
$\mathbf{z_2}$	Error state matrix

Chapter 1

Introduction

1.1 Motivation

Autonomy has emerged as a field of interest and research in the industry, mainly because of the many benefits it may yield to different aspects of the industrialized society. The possibility to solve complex tasks faster and more efficient, while reducing the risk of accidents and cutting operational costs is driving this research. According to Allianz (2017), written by one of the largest insurance companies in the world, human error is behind 75% of marine liability losses in the industry. Shipping and maritime operations could reap great benefits of autonomy, as cutting in costs and dependability of crew, or certain crew members, could save companies significant amounts of money.

Most ship voyages start and culminates in docking the ship in a harbor at a quay, an operation that can be critical and complex. Taking local phenomena, traffic, and environmental forces into account, the docking operation requires skill, teamwork, and sometimes even local knowledge and experience. A robust autonomous system could therefore be of great use, eliminating the human factor as well as being able to undertake such a mission in even more complex situations.

1.2 Objectives

The overall objective of this thesis is to design and develop an autonomous docking controller (ADC), utilizing a conventional sensor suite combined with proximity sensors. The main objective will be achieved by several intermediate objectives, listed below.

- Perform a literature review providing information and references on relevant topics.
- Decide on, and implement, a navigation system to provide the ADC with relevant information.
- Develop a guidance system utilizing the proximity sensors to plan and generate a desired path for the operation. Look into how to implement situational awareness and reactiveness based on the proximity sensor measurements.
- Decide on, and implement, a control system being able to perform path following and docking according the guidance system.
- Validate the ADC in simulations.

1.3 Scope

This thesis will focus on designing an autonomous docking system for a fully actuated ship, fitted with proximity sensors at the bow and stern on starboard side. The ADC is thought to take over the operation from an autonomous harbor maneuvering controller in proximity to the quay. The operation starts with positioning the ship for docking, and ends when the ship has stopped a desired distance from the quay side. Specific assumptions regarding the thesis will be touched upon in Chapter 3.

1.4 Thesis contribution

The contribution of this thesis is a complete autonomous docking controller utilizing traditional sensors aided by proximity sensors. This controller could be employed by vessels on a large scale, as it requires little to no modification of the vessel, and proximity sensors are relatively cheap to acquire and install. The main contribution from this thesis lies in the design of the guidance system which uses a path parametrized by path tangential and path normal variables, as well as the exploration in regards to situational awareness and reactiveness. Existing solutions are used for motion control, observer design, and path generation. A significant amount of time has been spent in MC-lab, testing, improving, and preparing the model ship C/S Enterprise and its thrusters and servos. The handbook for C/S Enterprise has been updated with new chapters and tutorials, as well as data from bollard pull tests. Also, proximity sensors has been fitted to C/S Enterprise for further experimentation in MC-lab.

1.5 Outline of thesis

The outline of the thesis is as follows:

- **Chapter 2** presents relevant background information on ship maneuvering and docking, ship sensors and instrumentation, navigation filter designs, methods for path generation, and motion control designs.
- **Chapter 3** is the problem formulation. This chapter presents the system and operation as a whole, the relevant reference frames and models, and components to be designed. The problem statements for each component will also be presented.
- **Chapter 4** presents the modeling of the proximity sensors which will be used in simulations.
- **Chapter 5** explains and presents the navigation system.
- **Chapter 6** explains and presents the guidance system. This includes path planning, path generation, the chosen guidance laws, and how situational awareness and reactiveness can be implemented by the use of proximity sensors.
- **Chapter 7** explains and presents the motion control system used for the whole operation, as well as a brief explanation of the thruster allocation.
- **Chapter 8** presents the model ship, and how the simulations were set up to correspond to the real life model ship. Preparatory work done in laboratory is also presented in this chapter.
- **Chapter 9** presents and discusses the results of the simulations.
- **Chapter 10** is the final conclusions of the thesis and suggestions for further work.

Chapter 2

Background

This chapter aims to provide information and background knowledge on the different aspects needed to design and implement an autonomous docking system, and will be a continuation of the preparatory project thesis work, Gauslaa (2019).

2.1 Ship maneuvering and docking

This section will provide background information regarding ship docking and maneuvering, the use of rudders and thrusters, docking speed, and accident causes. The information is mainly found in Murdoch et al. (2012), Fossen (2011) and Roubos et al. (2017), which gives extensive insight to these subjects, amongst others.

2.1.1 The golden rules of berthing

Murdoch et al. (2012) defines five golden rules, which should be kept in mind at all times before and during docking of a ship:

- Slow speed.
- Controlled approach.
- Planning.
- Teamwork.
- Checking equipment.

2.1.2 Accidents related to docking

In the work by Murdoch et al. (2012) several case studies are listed with a short explanation of the situation, followed by the cause and how it could have been avoided. The majority of the accidents can be attributed to mistakes done by individuals, and very often involves high

speeds. In many of the cases reviewed, lack of communication is to blame for the accident. Not repeating orders, not verbally handing over command of the ship, different equipment settings on different telegraphs, and language barriers are all examples of communication related errors which have led to ships hitting the quay. Other reasons for accidents are equipment failure, failure to understand the ship's characteristics, and failure to allow for environmental forces. Autonomy could help improve in several of these areas, as the human involvement in the process of docking can be decreased, or eliminated.

2.1.3 Ship factors affecting handling and maneuvering

The pivot point: When maneuvering a ship in tight spaces it is important to know which point the ship turns about. This point is called the pivot point, and it is the yaw rotation point of the ship. The pivot point lays on the centerline of the ship measured from the center of gravity, as stated by Fossen (2011). According to Murdoch et al. (2012) the position of the pivot point is a function of different influences. With headway, the pivot point is said to be between $\frac{1}{4}$ and $\frac{1}{3}$ of the ship's length from the bow. With sternway, the pivot point lay a corresponding distance from the stern. For a ship without speed through the waves, the position is dependent on the different forces acting on the body.

"The pivot point traces the path that the ship follows." - Murdoch et al. (2012)

Lateral motion: Because the pivot point is not located at the center of the ship, there will be lateral motion when turning, as described by Murdoch et al. (2012). An example of this is a ship with headway turning port, resulting in lateral movement to starboard. With sternway, the lateral motion is towards the way the ship turns. Understanding the pivot point and lateral motion can be crucial when navigating close to hazards, such as a quay or other ships.

Actuators: Ship motion can be manipulated using several different instruments. A rudder is one of the most common ways to turn a ship. A rudder is a hydrofoil fitted at the ship stern, which utilizes the long moment arm to the pivot point. The rudder is a passive instrument, and it is dependent on water passing over it to generate a lift force. This water flow is generated by the ship moving through the water and by the propeller jet. The rudder effectiveness is highly dependent on water flow. Low inflow speed, or obstacles like a stopped propeller in front of the rudder can reduce effectiveness. Rudder response time is also a limiting factor to how fast a ship can turn, as the rudder requires time to change position.

As an alternative to a conventional rudder and propeller combination, thrust vectoring devices such as Azimuth thrusters are also used. Azimuth thrusters work by directing the propeller slipstream. This may enhance maneuverability compared to a rudder, as all of the thrust is vectored. Azipods are also widely used. An azipod is an underwater streamlined pod, fitted with a propeller(s). Inside this pod sits an electric motor used to spin the

propeller. This pod can be rotated and therefore can act both as a propeller and rudder.

Lateral thrusters are also used for ship maneuvering. These can be fitted in the bow, or the stern. These lateral thrusters are most effective when the ship has zero forward speed through the water. Providing a lateral force, these thrusters can turn the ship and move in sway.

Approach speed and kick ahead: Many accidents happen because of the approach speed being too high. It is necessary to slow down before berthing, as transit and approach phases usually are done at different speeds. While slowing down or stopping, it is normal to set the engines astern, which drastically reduces the effectiveness of the rudder, and therefore can result in loss of steering. When the ship has come down to a very slow speed, maneuvering can be difficult due to low water inflow to the rudder. To turn the ship, the ship master can do a "kick ahead". A kick ahead is done by putting the engines ahead for a short burst, giving increased inflow to the rudder, but not long enough to overcome the ship longitudinal inertia resulting in zero forward speed.

2.1.4 Berthing under environmental influences

Wind: Wind can be a significant disturbance, and can cause both heading changes and drift in position. Therefore, it is important to take wind into account to ensure the robustness of the controller. How much a ship is influenced by wind is dependent on the geometry of the ship. Typically high-sided ships, or ships with a large frontal area towards the wind, will be more prone to the effects of wind. According to Murdoch et al. (2012) a ship is most vulnerable when the broadside is facing the wind.

Current: Depending on the direction of the current relative to the quay and ship, the current makes the act of berthing more complicated. If the current has direction towards the ship, parallel to the quay, it can be used to stop the ship. A head current also increases flow over the rudder, even though speed over ground (SOG) can be low. Berthing with a following current can drastically decrease maneuverability, as the engines will have to be set astern to stop the ship, decreasing flow over the rudder. When dealing with current not parallel with the quay, one has to keep in mind that a large angle between the current and quay may cause sideways motion. Use of thrusters can help prevent unwanted motion caused by current.

2.1.5 Hydrodynamic effects

Water depth: Water depth can also effect the maneuverability and speed of the ship. As the water gets shallower, resistance of the ship increases. Murdoch et al. (2012) states that as water depth decrease, so does the turning ability. As water is dragged along with the ship, the effect of the rudder can also decrease.

Waterway width: Like depth, the width of the waterway also has an effect on the ship.

First, a bank under water may increase the resistance and create a backflow of water between the ship and the waterway. Also, if the bank is high relative the water depth, the ship might steer away from the bank. This is due to a backflow between the ship and the bank, which creates a low-pressure region amidships. This low pressure sucks the ship in towards the bank, and pushes the bow out and the stern in towards the bank. The bank effect is increased with increasing speed and blockage. Blockage is the size of the cross-section of the ship relative to the cross section of the bank.

These hydrodynamic interaction forces are also present in relation to other ships. When a ship comes in proximity of another ship at a high enough speed, the ship may be drawn close to the other ship, or both ships might be turned away or towards each other.

To decrease the potential for these interaction forces, the ship master must anticipate the situation, and decrease speed.

2.1.6 Common docking procedures

Murdoch et al. (2012) writes about different berthing scenarios; with tugs, without tugs, and with the use of anchors. In this thesis the focus will be without tugs and anchors. The procedures will be considering a ship with several actuators, such as main propeller, rudder, and bow thrusters. For this ship the actuators can be used in different ways, and Murdoch et al. (2012) divides them in to two different methods.

Port-side docking: The first of which is only using rudder and main propeller, named "port-side docking". The way this is done is to approach the quayside at an angle and with appropriate speed, such that astern thrust can be used to stop the ship, push the bow out and the stern in, resulting in the ship laying parallel to the quay. It is important to remember and account for the interaction forces mentioned earlier, as this way of docking involves forward speed alongside the quay. Port side docking is illustrated in Figure 2.1a.

Docking with thrusters: The other method is utilizing thrusters to move the ship in sway towards the designated position alongside the quay. This is usually done by lining up the ship in the correct fore and aft position outside its designated position. The next step is to move the ship sideways towards the quayside by the use of thrusters. This method is illustrated in Figure 2.1b, with a ship docking in between two other ships.

When docking this way, it is important to consider the current. As the speed of the ship is small it is more affected by current than in the case of port-side docking. An alternative way to move the ship in parallel to the quay, is to move the bow or stern in towards the quayside first, followed by the other end.

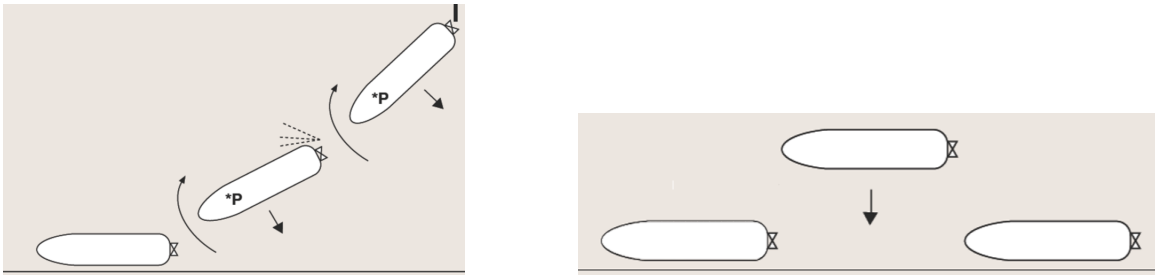

(a) Port-side docking.

(b) Docking with thrusters.

Figure 2.1: Docking procedures [Courtesy of Murdoch et al. (2012)].

2.1.7 Docking speed

Speed is amongst the most important factors when it comes to the safety and success of a docking operation. Roubos et al. (2017) has done extensive research on the docking speed of large seagoing vessels berthing in the port of Rotterdam. Containers, tankers, and bulk ships are examined, all of various sizes ranging from small feeders to ultra large container vessels (ULCVs). From 555 berthings, the mean docking speed was 4 cm/s and the maximum was 13 cm/s. Little to none correlation was found between the mass of a vessel and its docking speed.

2.2 Relevant ship sensors and instrumentation

In order to maneuver the ship safely to the correct destination, the system needs to gather information on its position, velocity, orientation, and surroundings. As the consequences have the potential of becoming very large in the event of an accident, the requirements for precise and accurate measurements and understanding of the ship and its surroundings are high. Sørensen (2018) divides the systems and sensors used by a positioning system into position reference systems and sensor systems.

Position reference systems: There are a variety of position reference systems, which are used to determine the position, and sometimes the orientation, of a ship. Some relevant position reference systems for this purpose are listed below.

- **Global Navigation Satellite Systems (GNSS):** One of the most widely used position reference systems is the US satellite navigation system, GPS. There are other GNSS providers with varying degrees of coverage depending on where in the world the user is situated. Examples are Glonass (Russian), Galileo (European), and Beidou (Chinese). These satellite systems use the principle of trilateration to determine the position of the receiver, and at least four satellites need to be above the horizon for it to work. At sea level this number can be reduced to three, as the height measurement will be sea level. Regular GPS typically has an accuracy of ±10 m. To receive even better accuracy one could use Differential GPS (DGPS) (±1 m), Carrier Differential GPS (CDGPS) (±0.1 m), or even Real-time Kinematic GPS (RTK GPS) (±0.01 m).
- **Hydroacoustic Position Reference (HPR) Systems:** This system consists of stationary transponders on the seabed, and transducers underneath the hull of the ship. The transducers emits an acoustic signal to the transponders, which replies back. Since the position of the transponders and the speed of sound through water is known, the position of the ship can be calculated. Different variations of such hydroacoustic systems are short baseline (SBL), ultra short baseline (USBL), and long baseline (LBL).
- **Radio navigation:** This concept revolves around radio beacons stationed on, or in near vicinity of the quay. A transmitter on the vessel transmits a signal to at least three beacons, which positions are known. The beacon then returns a signal, and from this signal the distance can be calculated from the time of flight, velocity from Doppler shift, and also angular directions. Kongsberg (n.d.b) presents such a system called RADius, made by Kongsberg. Wärtsilä also has a system called Artemis, used for relative positioning, Wärtsilä (n.d.).
- **Optical systems:** An example of an optical position reference system is Kongsberg's SpotTrack, Kongsberg (n.d.a), which is a laser-based position reference system. This system is used for relative positioning. The system consists of a housing contain-

ing rotating laser sensors that measures range and bearing to small reflective points installed on the target chosen as a relative platform, for example a quay.

Sensor systems:

- **Magnetic compass:** Uses the magnetic field of the earth to determine the direction of *magnetic* north.
- **Gyrocompass:** Uses a gyroscope and the rotation of the earth to determine the direction of *true* north, and the heading of the ship relative to it. As this device uses the effect of gyroscopic precession, it is not affected by ferromagnetic materials, which a magnetic compass will. As magnetic north is not stationary, and the earth's magnetic field is not homogeneous, a gyrocompass might be preferred over a magnetic compass.
- **Inertial Measurement Unit (IMU):** Uses gyroscopes, accelerometers and magnetometers to determine the specific force and angular rate of a body. This unit can take measurements for each axis, providing measurements in all degrees of freedom (DOFs). This type of sensor is typically used by an Inertial Navigation System (INS) to provide relative position, attitude, velocity, and angular rates. Can be utilized in a potential scenario of loss of signal from a GNSS to calculate position, also called dead reckoning.
- **Environmental sensors:** Wind sensor to measure the wind speed and direction, which can introduce a significant disturbance to the system. Often used in a feedforward loop such that the system can predict gusts of wind. Draft sensor to measure depth. Wave sensors to measure significant wave height, wave direction and frequency. Current sensors to measure velocity and direction of the current.
- **Acoustic Doppler current profiler (ADCP):** Uses the Doppler effect of sound waves scattered from particles in the water to measure current velocities. Can also be used for bottom tracking, as well as to calculate speed over ground.
- **Proximity sensors:** These are used to measure distance between the location of the proximity sensor and to an object in the sensor direction. Sonar, inductive, infrared and radar are examples of methods utilized by different proximity sensors.
- **Lidar:** (light detection and ranging) is an instrument used to measure distance by illuminating the target with light, and measuring the reflected light. This can be used to create a 3D-mapping of an object or the surroundings of the instrument itself.
- **Radar:** (radio detection and ranging) uses radio waves to measure distance, angle or velocity. The reflection time of the radio signal is used to calculate distance or velocity.

Usually, class rules dictate what sensors and measurements should be available, depending

on the ship and the mission it is to undertake. Redundancy are also dependent on the mission complexity, as this increases the safety and availability of the systems. One could also integrate different sensor systems and position reference systems to increase precision and accuracy.

2.3 Relevant navigation filter designs

To process sensor and navigation data, motion control systems use a navigation system. The main function of the navigation system is to filter out noise on the measurements, prediction, and reconstruction of unmeasured states. The signal provided by the observer is used by control and guidance systems. Fossen (2011) discusses several filters and observers. The environmental forces are considered disturbances to the motion of the control system, and can be divided into low-frequency and wave-frequency components. Only low-frequency motion should be compensated for by the steering and propulsion systems, due to the risk of wear and tear, as well as increased fuel consumption.

There are mainly two different type of observers, stochastic and deterministic. A stochastic approach considers the vehicle model with uncertainties and uses a stochastic state estimator. The deterministic approach uses sensors, e.g. accelerometer measurements, directly in the motion model, this is typical for INS, and is independent of the vehicle. It is an advantage that a system is independent of the vehicle model, as it is easier to apply the same observer to different vessels. One of the big advantages of the stochastic approach is the ability to be used as a predictor if GPS measurements fail, enabling dead reckoning. In a critical operation such as docking, redundancy is needed, and dead reckoning could be one way to handle an event of loss of signal.

2.3.1 Lowpass, highpass and bandpass filters

The idea behind lowpass filters are to only let through signals lower than a defined threshold frequency. A highpass filter is meant to let through frequencies higher than a defined threshold. The two aforementioned filters can be combined to create a bandpass filter, only letting through signals in a defined interval.

2.3.2 Kalman filter

A widely used stochastic filter is the Kalman filter (KF), which is discussed in Fossen (2011, chap. 11.3). The Kalman filter is named after Rudolf Emil Kálmán, the main developer behind its theory, and is presented in Kálmán (1960). The KF has been widely applied in engineering projects since the 1960s, and examples are the Apollo project, weapon systems, and civilian navigation and guidance systems. The KF is a recursive filter that estimates the real states from noisy measurements. It is able to both reconstruct unmeasured states, and remove noise from the state estimates. In the case of loss of signal from either sensors

or GNSS, the KF behaves as a predictor enabling dead reckoning. The Kalman filter can be applied to nonlinear systems as well, in the form of the extended Kalman filter (EKF), which linearizes about an estimate of the current mean and covariance.

2.3.3 Nonlinear passive observer

When the EKF is used together with a linear quadratic controller or proportional-integral-derivative controller (PID), the nonlinear system can not be guaranteed stable (Sørensen; 2018). A globally stable deterministic observer, the nonlinear passive observer (NPO), is proposed in Fossen (2000), but can also be found Fossen (2011). At the time, existing dynamic positioning (DP) systems used Kalman filters for state estimation and wave filtering. These Kalman filters were linearized around predefined constant yaw angles, typically at 10 degree intervals, resulting in 36 operating points. This results in a time consuming and difficult tuning process, motivating the development of the NPO. The NPO reduces the observer gains to only one set covering the whole state space, and is based on the passivity arguments:

1. Zero mean white noise terms are neglected, $\boldsymbol{w} = 0$, and $\boldsymbol{v} = 0$.
2. $\boldsymbol{R(y_3)} = \boldsymbol{R(\psi)}$ which indicates that $y_3 = \psi + \psi_w \approx \psi$.

The last assumption can be done due to the fact that the wave-induced yaw disturbance, ψ_m, is small, usually less than 1° under normal operation.

2.4 Path generation

Given a set of waypoints (WPs), a path for the vessel to follow must be generated. There are several ways of doing this, and some are presented in Skjetne (2005) and Fossen (2011). Lekkas (2014) also provides an extensive look into different techniques and methods. Among the methods of generating paths from waypoints are:

- linear path segments,
- the combination of linear path segments and arc segments,
- spline interpolation techniques.

It is desirable to generate a smooth path, such that there are no jumps in the signal sent to the control system at each waypoint. By having a path parametrized by linear segments connected at the waypoints, one will find a discontinuity in each WP, resulting in a jump in the desired signal. By combining circular arcs and straight lines, Dubins (1957) made a continuous path connecting the waypoints, but which still results in a jump in the desired yaw rate.

By using spline interpolation techniques, a curve is constructed through a given set of waypoints. Several interpolation methods exists. One method that avoids the jump in yaw rate experienced by Dubins, is mentioned in Fossen (2011) as cubic spline interpolation. Cubic spline interpolation requires the second order derivatives at the endpoints of the polynomials to be equal, ensuring a smooth spline. Fossen (2011) presents methods to interpolate a cubic spline by considering cubic polynomials. Other interpolation methods, such as the hybrid path parametrization, can be found in Skjetne (2005).

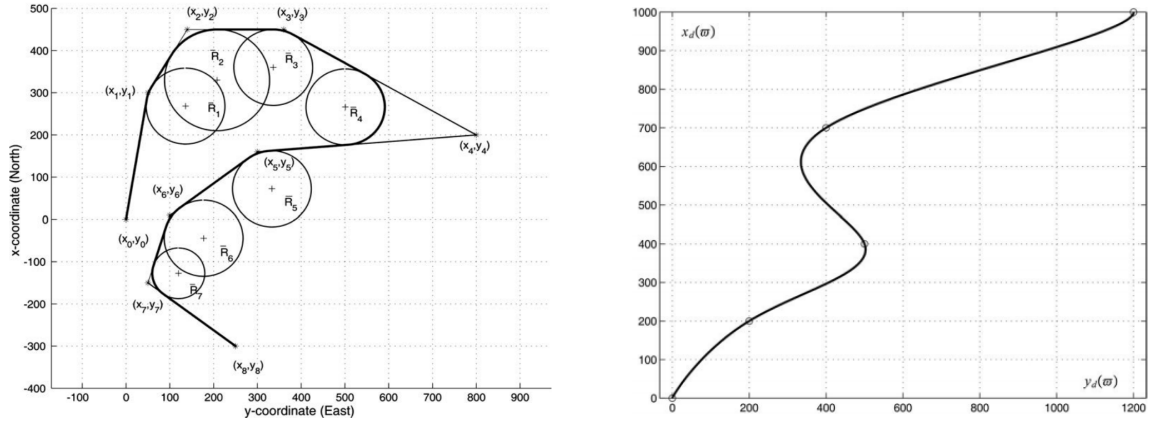

(a) Dubins.

(b) Cubic spline.

Figure 2.2: Examples of both Dubins and cubic spline interpolation [Courtesy of Fossen (2011)].

2.5 The maneuvering problem and maneuvering control designs

To make the vessel behave according to for example a desired speed or heading, one or more motion controllers are needed to calculate the appropriate and desired actuator outputs. Skjetne (2005) formulates the problem to be solved by the motion controller as "the maneuvering problem". The maneuvering problem consists of two tasks, a geometric and a dynamic task. The geometric task is to follow a desired path, and the dynamic task could be either a time, speed, or acceleration assignment that the vessel is to follow. Several different motion control designs can be utilized to solve the maneuvering problem.

2.5.1 PID controller

A simple controller, which was used in early applications of vessel steering and control is presented in Fossen (2011) as a proportional–integral–derivative controller. The PID-controller in marine applications dates back to 1922, when Nicolas Minorsky proposed to apply PID controllers to the directional steering system of ships in Minorsky (1922). The PID controller is a model free controller, and is based on applying a correction calculated from the error between the desired setpoint and the measured variable, based on proportional, integral, and derivative gains.

2.5.2 Backstepping controller

Another type of controller can be found in Skjetne (2019a), Skjetne (2005), and Fossen (2011), called backstepping maneuvering controller. Several different designs are presented. The idea of backstepping control designs started to emerge in the late 1980s and 1990s according to Fossen (2011). Backstepping makes a feedback control law by recursively constructing a control Lyapunov function (CLF) to prove stability. In addition to this, another type of backstepping controller can be found in Skjetne (2020) as a cascaded backstepping controller. This method rely on cascaded systems theory to prove stability, and individually design controls for the subsystems instead of recursively building a CLF.

Chapter 3

Problem formulation

3.1 System description

The aim of this thesis is to develop an autonomous docking controller, considering a fully-actuated autonomous surface vehicle (ASV), enabled with DP functionality. The ADC is thought to gain control of the ship when in proximity of the dock, after the ship has been maneuvered through the harbor to its designated docking area. The docking operation will be divided into two phases, and is considered a low-speed operation.

Phase 1 will be to align the ship outside its designated docking spot, parallel to the dock. Starting in the position the ship has when activating the ADC, waypoints and a path are made to a point outside the dock. This path is then followed by a DP system. The heading should be parallel to the dock at the end point. Environmental forces such as current, waves, and wind can affect the ship greatly during this phase, resulting in unwanted motion.

Phase 2 will be to generate a docking path, and move the ship towards the quay in sway according to this path. This should be done in a controlled fashion and the ship should stop at a desired distance from the quay without collision. Maintaining a low speed and correct heading is an important safety measure. The ship should be parallel to the dock during Phase 2. In addition to the environmental forces in Phase 1, interaction forces between the ship and the quay wall may affect the ship.

The whole operation is illustrated in Figure 3.1.

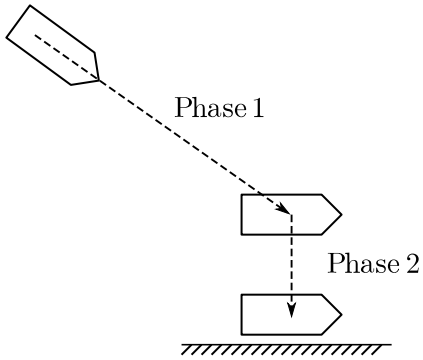

Figure 3.1: Docking operation overview.

Waypoints should be placed automatically between the start point and a point outside the designated docking spot. The position of the dock and the position of the ship are assumed known, and a path connecting the waypoints have to be generated. This path must be smooth and sufficiently differentiable. It is imperative that the docking operation is done in a safe manner. There should be minimal risk for accidents and material and/or human damage. Proximity sensors mounted on the ship side will be used to measure the distance from the ship to the dock, in addition to GNSS and compass providing x, y, and yaw (ψ) measurements, $\boldsymbol{\eta} = [x, y, \psi]^\top$.

Assumptions

The following assumptions will be applied to the thesis:

- The vessel model parameters are known.
- Fully actuated ship - enabling DP functionality.
- No environmental forces other than current.
- Low-speed operation.
- Perfect GNSS and sensor measurements, apart from measurement noise.
- Static dock - the position of the dock is fixed.
- Straight dock edge.
- The ADC is part of a bigger autonomous system with a path planner that lets the ADC start with the ship heading tangential to the first path segment.

Design and simulation tools

Matlab and Simulink will be the tools utilized for design and development of the ADC, as well as simulating the system to test and verify it.

3.2 Modeling

3.2.1 Reference frames

Two different reference frames will be used when describing the kinematics of a marine vessel, the NED and body frame.

North-East-Down frame

The North-East-Down (NED) frame, denoted {n}, is defined as a tangential reference frame relative to the earth surface, and is used for local navigation. Assuming constant longitude and latitude, this reference frame is assumed to be inertial, and Newton's laws apply. A vessel's position and orientation is expressed in NED. This reference frame moves with the vessel, with its x-axis pointing true north, y-axis to the east and z-axis downwards towards the center of the earth.

Body frame

The body fixed reference frame, denoted {b}, is a reference frame fixed to the vessel. The body frame is used to express positions on the vessel, linear and angular velocities of the vessel, and forces acting on the vessel. In this frame, the x-axis points along the longitudinal direction of the vessel, y-axis in the starboard direction, and the z-axis is the normal axis.

3.2.2 Simulation model

To get an accurate representation of the vessel dynamics and behavior in 6DOF, a high fidelity model is needed. This model is usually called *process plant model* or *simulation model*. The simulation model will be used to simulate the plant during simulation testing. The kinetic model from Fossen (2011) as shown below, will be used as a simulation model in this thesis.

$$\dot{\boldsymbol{\eta}} = \mathbf{J}_{\boldsymbol{\Theta}}(\boldsymbol{\eta})\boldsymbol{\nu} \tag{3.1a}$$

$$\mathbf{M}\dot{\boldsymbol{\nu}} + \mathbf{C}(\boldsymbol{\nu}_r)\boldsymbol{\nu}_r + \mathbf{D}(\boldsymbol{\nu}_r)\boldsymbol{\nu}_r + \mathbf{g}(\boldsymbol{\eta}) = \boldsymbol{\tau} + \boldsymbol{\tau}_{\text{wind}} + \boldsymbol{\tau}_{\text{wave}}, \tag{3.1b}$$

with $\boldsymbol{\eta} = [x, y, z, \phi, \theta, \psi]^\top \in \mathbb{R}^3 \times \mathcal{S}^3$ representing position and orientation in NED-frame. The body fixed linear and angular velocities in body frame is given by $\boldsymbol{\nu} = [u, v, w, p, q, r]^\top \in \mathbb{R}^6$, while the forces acting on the body is represented by $\boldsymbol{\tau}$. The relative velocity between the vessel and the water is given as $\boldsymbol{\nu}_r = \boldsymbol{\nu} - \boldsymbol{\nu}_c$, where $\boldsymbol{\nu}_c$ is the current velocity. The restoring forces are given by $\mathbf{g}$, while the system inertia matrix, $\mathbf{M}$, Coriolis-centripetal

matrix, $\mathbf{C}$, and damping matrix, $\mathbf{D}$ are given by

$$\mathbf{M} = \mathbf{M}_{\mathrm{RB}} + \mathbf{M}_{\mathrm{A}} \tag{3.2a}$$

$$\mathbf{C}(\boldsymbol{\nu}_r) = \mathbf{C}_{\mathrm{RB}}(\boldsymbol{\nu}_r) + \mathbf{C}_{\mathrm{A}}(\boldsymbol{\nu}_r) \tag{3.2b}$$

$$\mathbf{D}(\boldsymbol{\nu}_r) = \mathbf{D} + \mathbf{D}_{\mathrm{n}}(\boldsymbol{\nu}_r), \tag{3.2c}$$

with $\mathbf{M}_{RB}$ and $\mathbf{C}_{RB}$ denoting the rigid body component, and $\mathbf{M}_A$ and $\mathbf{C}_A$ denoting an added component due to the acceleration of water. Also, $\mathbf{J}_\Theta(\boldsymbol{\eta})$ is given by

$$\mathbf{J}_\Theta(\boldsymbol{\eta}) = \begin{bmatrix} \mathbf{R}_b^n(\Theta_{nb}) & 0_{3x3} \\ 0_{3x3} & \mathbf{T}_\Theta(\Theta_{nb}) \end{bmatrix}, \tag{3.3}$$

with $\mathbf{R}_b^n(\Theta_{nb})$ and $\mathbf{T}_\Theta(\Theta_{nb})$ expressed as

$$\mathbf{R}_b^n(\Theta_{nb}) = \begin{bmatrix} \cos\psi\cos\theta & -\sin\psi\cos\phi + \cos\psi\sin\theta\sin\phi & \sin\psi\sin\phi + \cos\psi\cos\phi\sin\theta \\ \sin\psi\cos\theta & \cos\psi\cos\phi + \sin\phi\sin\theta\sin\psi & -\cos\psi\sin\phi + \sin\theta\sin\psi\cos\phi \\ -\sin\theta & \cos\theta\sin\phi & \cos\theta\cos\phi \end{bmatrix}, \tag{3.4}$$

and

$$\mathbf{T}_\Theta(\Theta_{nb}) = \begin{bmatrix} 1 & \sin\phi\tan\theta & \cos\phi\tan\theta \\ 0 & \cos\phi & -\sin\phi \\ 0 & \sin\phi/\cos\theta & \cos\phi/\cos\theta \end{bmatrix}. \tag{3.5}$$

3.2.3 Control design model

The 3DOF control design model for a DP vessel is a simplified model of the vessel dynamics, and is sufficient for a control objective. By assuming that $w \approx \phi \approx \theta \approx 0$, heave, roll, and pitch dynamics can be neglected. For low speed applications, linearized about zero speed, a model is presented in Skjetne (2005) as

$$\dot{\boldsymbol{\eta}} = \mathbf{R}(\psi)\boldsymbol{\nu}, \tag{3.6a}$$

$$\mathbf{M}\dot{\boldsymbol{\nu}} + \mathbf{D}\boldsymbol{\nu} = \mathbf{R}(\psi)^\top \mathbf{b} + \boldsymbol{\tau}, \tag{3.6b}$$

where the vessel position and heading $\boldsymbol{\eta} = [x, y, \psi]^\top \in \mathbb{R}^2 \times \mathcal{S}$, and the bias, $\mathbf{b}$, are given in the NED-frame, whereas vessel speed and yaw rate, $\boldsymbol{\nu} = [u, v, r]^\top \in \mathbb{R}^3$, as well as the control forces and moment, $\boldsymbol{\tau} = [X, Y, N]^\top$, are given in the vessel body reference frame. Transition between the two frames is performed through the rotation matrix $\mathbf{R}(\psi)$. The vessel inertia matrix $\mathbf{M}$, the damping matrix $\mathbf{D}$, and the correolis matrix $\mathbf{C}$ are given as:

$$\mathbf{M} = \begin{bmatrix} m - X_{\dot{u}} & 0 & 0 \\ 0 & m - Y_{\dot{\nu}} & mx_g - Y_{\dot{r}} \\ 0 & mx_g - Y_{\dot{r}} & I_z - N_{\dot{r}} \end{bmatrix} = \mathbf{M}^\top > 0, \tag{3.7}$$

and

$$\mathbf{D} = \begin{bmatrix} d_{11} & 0 & 0 \\ 0 & d_{22} & d_{23} \\ 0 & d_{32} & d_{33} \end{bmatrix}, \tag{3.8}$$

where d_{ij} are the damping components for the respective directions. The hydrodynamic coefficients of $\mathbf{M}$ are presented in Chapter 8. $\mathbf{M}$ and $\mathbf{D}$ for CSEI can be found in NTNU (2020). Furthermore, the rotation matrix $\mathbf{R}(\psi)$ is given by:

$$\mathbf{R}(\psi) = \begin{bmatrix} \cos\psi & -\sin\psi & 0 \\ \sin\psi & \cos\psi & 0 \\ 0 & 0 & 1 \end{bmatrix}. \tag{3.9}$$

It is noted that

$$\mathbf{R}(\psi)^\top \mathbf{R}(\psi) = \mathbf{R}(\psi)\mathbf{R}(\psi)^\top = \mathbf{I}, \tag{3.10a}$$

$$\dot{\mathbf{R}}(\psi) = \dot{\psi}\mathbf{R}(\psi)\mathbf{S}, \qquad \mathbf{S} = -\mathbf{S}^\top, \tag{3.10b}$$

with

$$\mathbf{S}_2 = \begin{bmatrix} 0 & -1 \\ 1 & 0 \end{bmatrix}, \qquad \mathbf{S} = \begin{bmatrix} \mathbf{S}_2 & 0_{2x1} \\ 0_{1x2} & 0 \end{bmatrix}. \tag{3.10c}$$

To rotate a point in one reference frame to another, $\mathbf{R}_2(\psi)$ will be used,

$$\mathbf{R}_2(\psi) = \begin{bmatrix} \cos\psi & -\sin\psi \\ \sin\psi & \cos\psi \end{bmatrix}. \tag{3.11}$$

Later, the skew symmetric matrix $\mathbf{S}$ will be used.

3.3 Problem statement

3.3.1 System overview

When designing and developing the ADC, the problem will be split into three main components. These components will be called "Navigation system", "Guidance system", and "Control system". The overall system is illustrated in Figure 3.2.

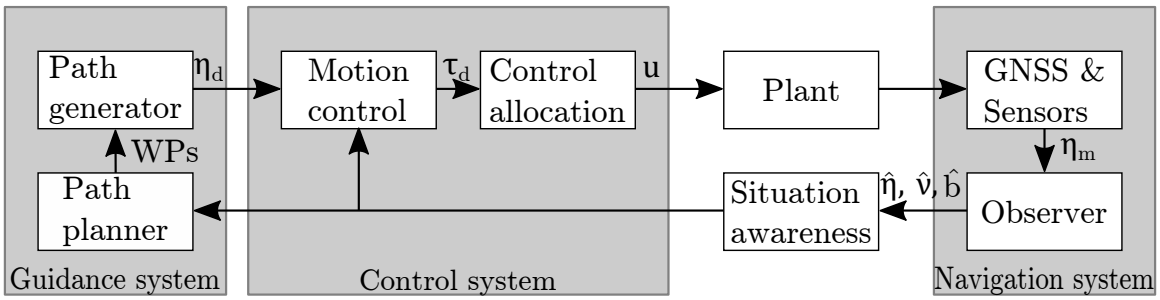

Figure 3.2: ADC components. Adapted from Fossen (2011).

In Figure 3.2, $\boldsymbol{\eta_m}$ are the measured position and heading, $\hat{\boldsymbol{\eta}}$, $\hat{\boldsymbol{\nu}}$, and $\hat{\mathbf{b}}$ are the estimated states, $\boldsymbol{\eta_d}$ are the desired position and heading, $\boldsymbol{\tau_d}$ are the desired forces and moment, and $\mathbf{u}$ are the thruster inputs. In the sections below, each component will be discussed, and a problem statement will be presented.

3.3.2 Navigation system

Observer

Measurements suffer from measurement noise and 1^{st}-order wave-induced wave frequency motions which has to be filtered out to avoid the actuators compensating for other than low frequency motion, due to the risk of wear and tear. The estimated motion is given by

$$\hat{\boldsymbol{\eta}} = \boldsymbol{\eta_m} - \boldsymbol{\eta_w} - \boldsymbol{v}, \tag{3.12}$$

where $\boldsymbol{\eta_m} = \boldsymbol{\eta} + \boldsymbol{\eta_w} + \boldsymbol{v}$, with $\boldsymbol{\eta_w}$ being the 1^{st}-order wave-induced wave frequency motions, and $\boldsymbol{v}$ being zero-mean Gaussian white measurement noise. As this thesis assumes no waves, $\boldsymbol{\eta_w}$ is assumed to be equal to zero.

In addition to the measurement noise filtering, the control system requires state information that are not measured directly, and thus has to be estimated. States that are needed but not measured directly is in this case the velocities $\boldsymbol{\nu} = [u, v, r]^\top$ and the bias, $\mathbf{b}$, of the system. The bias comes from 2^{nd}-order wave drift forces, current and model uncertainties. The observer is tasked with this state estimation and noise filtering.

In addition to this, it is imperative that the estimated states are as close to the real states

as possible, resulting in the problem statement

$$\lim_{t\to\infty} |\boldsymbol{\eta}(t) - \hat{\boldsymbol{\eta}}(t)| = 0. \tag{3.13}$$

3.3.3 Guidance system

The guidance system is to provide a trajectory for the vessel to follow. Being fed with output from the navigation system, it will first make a set of waypoints, then a trajectory connecting these will be generated.

Path planner

The path planner will generate a set of waypoints, $\mathcal{WP}$, in the two dimensional workspace, starting from position of the ship, p_0, to the target position, p_n,

$$\mathcal{WP} = \{p_0, p_1, ..., p_n\} \tag{3.14}$$

Each WP consists of coordinates in the horizontal plane, $p_k = [x_k, y_k]^\top$ for $k = \{0, 1, ..., n\}$ where n is the number of waypoints.

Path generator

Waypoints are sent to the path generator which will generate a trajectory for the ship to follow, connecting the waypoints. The generated trajectory must be smooth, and continuously differentiable. It must also be differentiable of a sufficient degree, k,

$$\mathbf{p_d}(s) \in \mathcal{C}^k. \tag{3.15}$$

The desired path, parametrized by s, $\mathbf{p_d}(s)$ will be given by

$$\mathbf{p_d}(s) = \begin{bmatrix} x_d(s) \\ y_d(s) \end{bmatrix}. \tag{3.16}$$

The path generator also defines the desired heading, ψ_d, along the generated path. During path following, this is typically set to be path tangential. During Phase 2 however, the heading should be parallel to the dock. The generated path and the desired heading is combined to form the desired position and heading signal

$$\boldsymbol{\eta_d} = \begin{bmatrix} \mathbf{p_d} \\ \psi_d \end{bmatrix}. \tag{3.17}$$

3.3.4 Control system

Motion control

Receiving data from the observer, as well as the desired path from the path generator, the motion controller is tasked with calculating the correct desired forces and moment from the actuators. The calculated desired forces should move the ship according to the desired trajectory and heading, at a desired speed. The desired forces and moment, $\boldsymbol{\tau_d} = [X_d, Y_d, N_d]$, is then sent to the control allocation. The problem statement of the motion controller is formulated as a maneuvering problem, divided into a geometric and a dynamic task as in Skjetne (2005).

1. **Geometric task:** forcing the output $\boldsymbol{\eta}$, for any continuous function $s(t)$ to converge to the desired path $\mathbf{p_d}(s)$, and desired heading ψ_d,

$$\lim_{t\to\infty} |\boldsymbol{\eta}(t) - \boldsymbol{\eta_d}(s)| = 0, \tag{3.18}$$

   with $\boldsymbol{\eta_d}(s) = [\mathbf{p_d}^\top, \psi_d]^\top$.

2. **Dynamic task:** to satisfy a desired dynamic behavior along the path. Depending on the mission or preference, this could be either a time assignment, a speed assignment, or an acceleration assignment. As time is not viewed as a constraint in this thesis, and the speed is viewed as an important safety factor, a speed assignment will be chosen. Having a continuous parametrized path $\mathbf{p_d}(s)$, $\upsilon_s(s,t)$ could be treated as a desired speed for $\dot{s}$. A speed assignment is used to force the speed, $\dot{s}$, along the path to converge to $\upsilon_s(s,t)$,

$$\lim_{t\to\infty} |\dot{s}(t) - \upsilon_s(s,t)| = 0. \tag{3.19}$$

Chapter 4

Proximity sensor modeling

To provide local measurements on the distance from the ship side to the dock, proximity sensors will be used. The proximity sensors will have to be modeled in the simulations, which will be done as shown in this chapter. The two sensors are placed on the starboard side of the ship, with sensor 1 in the bow and sensor 2 at the stern.

Letting $p = [x, y]^\top$ denote the position of the ship in the global reference frame, and $p^b_{s_i} = [x^b_{s_i}, y^b_{s_i}]^\top$ for $i = 1, 2$ denote the position of the proximity sensors in body frame, the position of the proximity sensors in the global frame is found by $p_{s_i} = p + \mathbf{R}_2(\psi)p^b_{s_i}$. A line extending perpendicularly to the ship side out from each proximity sensor is constructed on the form $f_{s_i} = a_{s_i}x + b_{s_i}$. The lines f_{s_i} are made by the use of linear regression on the points p_{s_i} and $p_{s_i} + \mathbf{N}_s$, with $\mathbf{N}_s$ being the normal vector to the line between the two sensors, this ensures f_{s_i} is perpendicular to the ship side. Letting $f_{dock} = a_{dock}x + b_{dock}$ denote a line representing the straight dock wall, the intersection point, p_{int_i}, of f_{s_i} and f_{dock} is found by setting $f_{s_i} = f_{dock}$. The distance from each sensor to the dock, d_i, is given by $d_i = |p_{int_i} - p_{s_i}|$.

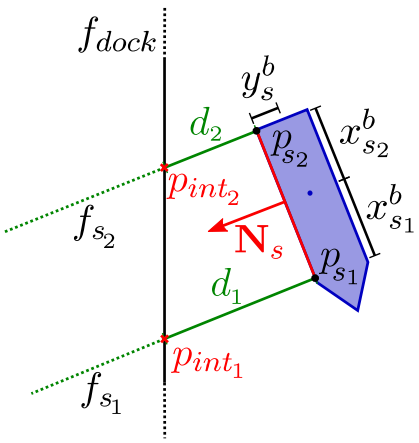

Figure 4.1: Explanatory figure for proximity sensor modeling.

Chapter 5

Navigation system

The navigation system consists of sensors and information processors, such as filters and/or observers. An observer is an important instrument, with several functions. The observer is tasked with filtering out noise on the sensor readings, reconstructing unmeasured states for use in a feedback control loop, and dead reckoning in the event of sensor failure.

5.1 Nonlinear passive observer

There exists many observer designs, some of which are mentioned in chapter 2. The chosen observer in this thesis will be the nonlinear passive observer presented in Fossen (2000) and Fossen (2011). The NPO has fewer tuning parameters than for example an EKF, and also has a guaranteed global convergence for estimation errors to zero. The observer presented is slightly modified, removing the wave filtering equations as environmental wave loads are not considered,

$$\dot{\hat{\boldsymbol{\eta}}} = \mathbf{R}(\mathbf{y_3})\hat{\boldsymbol{\nu}} + \mathbf{K_2}\tilde{\mathbf{y}}, \tag{5.1a}$$

$$\dot{\hat{\mathbf{b}}} = \mathbf{K_3}\tilde{\mathbf{y}}, \tag{5.1b}$$

$$\mathbf{M}\dot{\hat{\boldsymbol{\nu}}} = -\mathbf{D}\hat{\boldsymbol{\nu}} + \mathbf{R^T}(\mathbf{y_3})\hat{\mathbf{b}} + \boldsymbol{\tau} + \mathbf{R^T}(\mathbf{y_3})\mathbf{K_4}\tilde{\mathbf{y}}, \tag{5.1c}$$

$$\hat{\mathbf{y}} = \hat{\boldsymbol{\eta}}. \tag{5.1d}$$

Here $\hat{\boldsymbol{\eta}}, \hat{\boldsymbol{\nu}}$ and $\hat{\mathbf{b}}$ are the estimated states, and $\boldsymbol{\tau}$ is the applied forces and moment from the actuators. The measurement vector is $\mathbf{y} = [x, y, \psi]^\top$, with $\tilde{\mathbf{y}}$ being the estimation error $\mathbf{y} - \hat{\mathbf{y}}$. $\mathbf{K_i} \in \mathbb{R}^{3x3}$ with $i = 2, 3, 4$, are observer gain matrices. Tuning rules for $\mathbf{K_i}$ are

proposed in Fossen (2011), knowing that

$$\mathbf{K_2} = \text{diag}(k_{21}, k_{22}, k_{23}), \tag{5.2a}$$

$$\mathbf{K_3} = \text{diag}(k_{31}, k_{32}, k_{33}), \tag{5.2b}$$

$$\mathbf{K_4} = \text{diag}(k_{41}, k_{42}, k_{43}), \tag{5.2c}$$

the diagonal elements of $\mathbf{K_2}$ are given by

$$k_i = \omega_{ci}, \qquad (i = 21, 22, 23), \tag{5.3a}$$

where $\omega_{ci} > \omega_{0i}$ is the filter cut-off frequency, ω_{0i} is usually set equal to the wave peak frequency. The remaining gain matrices $\mathbf{K_3}$ and $\mathbf{K_4}$ are proposed to be

$$1/T_i << k_{3i}/k_{4i} < \omega_{0i} < \omega_{ci}, \qquad (i = 1, 2, 3). \tag{5.4}$$

With a tuned and properly functioning navigation system, a guidance and control system requiring information from this can now be made.

Chapter 6

Guidance system

As stated in Chapter 3, the guidance system is tasked with generating appropriate waypoints for the vessel, and a feasible path from these. The guidance system should generate both desired position and heading, $\boldsymbol{\eta_d}$. In this chapter the approach to how many WPs and the placement of these, a path generating approach and guidance laws will be decided. The path and desired position and heading will be used as input for the motion controller, which is tasked with calculating the desired thruster forces and moment such that Equation 3.18 is satisfied.

6.1 Path planning

The docking method of choice will we be the "docking with thrusters"-method from Chapter 2. Assuming that the harbor maneuvering controller (be it autonomous or humanly operated) will maneuver the vessel to the docking area, the ADC should take over operations within the docking area. The path planning algorithm should plan a path that can be used during both Phase 1 and Phase 2 without replanning when transitioning phases, and enable a safe and accurate docking by placing n number of waypoints.

As the vessel is thought to move along the normal vector of the entry path to the last WP, p_n, during Phase 2, the last path segment should be approximately parallel to the dock. This also implies that the last WP is at the end of Phase 1, outside the designated docking position. To achieve near parallel entry to p_n, $p_{(n-1)}$ must be at approximately the same lateral distance from the quay as p_n. As space for large maneuvers might be restricted in harbors and near quay, it is also desirable to avoid unnecessarily sharp turns.

It is assumed that the position of the ship and the position of the quay is known, so the path planner should take these as inputs when calculating where to place the WPs. By placing p_n a specified distance outside the designated docking spot, $p_{(n-1)}$ can be placed a given distance behind p_n at approximately the same distance from land, ensuring a near-parallel

last path segment. By placing at least one WP between the start position, p_0, and $p_{(n-1)}$, the change in heading between path segment N and $N-1$ can be reduced. In the figures below, different number of waypoints and placement of these will be shown, with the normal vector of the last path segment extending out from the last WP.

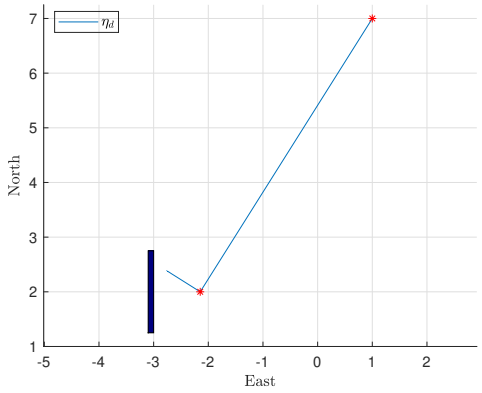

(a) Only start and end WP.

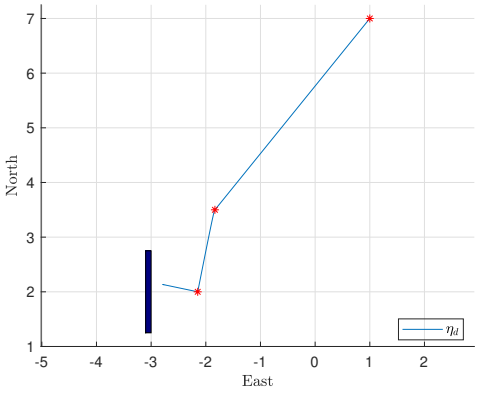

(b) One additional WP.

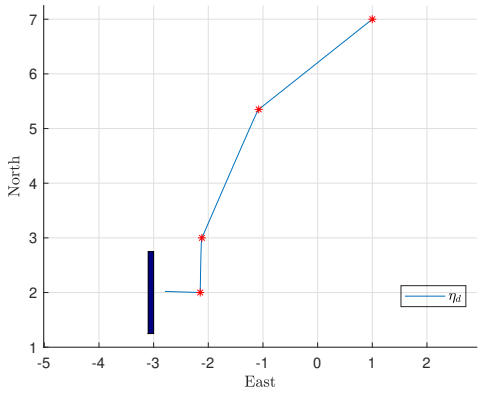

(c) Adding a WP to ensure normal vector perpendicularity to dock.

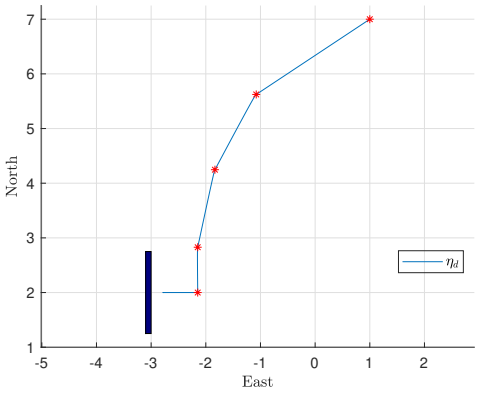

(d) Adding a WP to reduce heading change on each path segment.

Figure 6.1: Different path planning algorithms, with increasing number of waypoints and tighter constraint on the perpendicularity of the normal vector and the dock.

As can be seen in Figure 6.1d, the additional waypoints compared to figure Figure 6.1b decrease the change of heading during each path segment, and the added WP $p_{(n-1)}$ ensures a dock-perpendicular normal vector for Phase 2. An approach as in Figure 6.1d is chosen as the waypoint planning for this thesis, resulting in 4 waypoints in addition to the initial position, p_0.

To decide where to place the points between p_3 and p_0 the distance along the x-axis (Δ_x) and y-axis (Δ_y) is used, together with coefficients deciding where along that distance the point is to be placed. Point p_4 will be placed a specified distance, d_{ph1}, out from the dock,

specifying how far out from the dock the vessel is at the end of Phase 1. Point p_3 will be placed the same lateral distance from the dock as p_4, but a specified distance, d_{tang}, behind. This results in the following equations, also accounting for the dock potentially having an angle offset ϕ_{dock} relative to the global coordinate system:

$$p_4 = p_{dock} + \mathbf{R}_2^\top(\phi_{dock}) \begin{bmatrix} 0 \\ d_{ph1} \end{bmatrix}, \tag{6.1a}$$

$$p_3 = p_4 + \mathbf{R}_2^\top(\phi_{dock}) \begin{bmatrix} d_{tang} \\ 0 \end{bmatrix}, \tag{6.1b}$$

$$p_2 = p_3 + \mathbf{R}_2^\top(\phi_{dock}) \begin{bmatrix} c_{2,x}\Delta_x \\ c_{2,y}\Delta_y \end{bmatrix}, \tag{6.1c}$$

$$p_1 = p_3 + \mathbf{R}_2^\top(\phi_{dock}) \begin{bmatrix} c_{1,x}\Delta_x \\ c_{1,y}\Delta_y \end{bmatrix}, \tag{6.1d}$$

$$p_0 = \begin{bmatrix} x_0 \\ y_0 \end{bmatrix}. \tag{6.1e}$$

The chosen constants and coefficients are given in Table 6.1. x_0 and y_0 are the ship initial position at the time of activating the ADC. Plots for different dock offset angles using the values in the table below can be seen in Figure 6.2.

Table 6.1: Constants and coefficients

Parameter	Definition	Value
d_{ph1}	Distance from dock to p_4	$3B$
d_{tang}	Distance from p_3 to p_4	$0.75L$
$c_{1,x}$	Distance coefficient in x for p_1	0.66
$c_{1,y}$	Distance coefficient in y for p_1	0.33
$c_{2,x}$	Distance coefficient in x for p_2	0.33
$c_{2,y}$	Distance coefficient in y for p_2	0.10

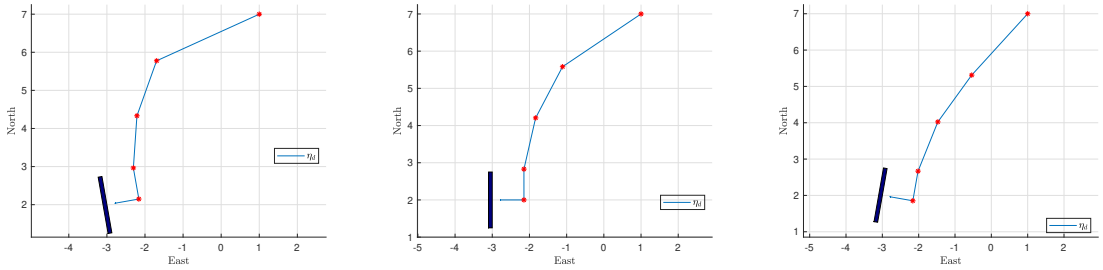

(a) Dock offset angle -10°. (b) Dock offset angle 0°. (c) Dock offset angle 10°.

Figure 6.2: Path planning with same inital position but with different dock offset angles.

6.2 Path generation

To generate a path from the decided WPs, a hybrid path parametrization as described in Skjetne (2005) will be used. This method constructs path segments of order r, that are concatenated at each WP such that the overall path is continuous and sufficiently differentiable. The path is parametrized by a path variable $s \in [0, N]$ with $N = n - 1$ being number of subpaths, and n being number of waypoints.

6.2.1 A $\mathcal{C}^r$ path generated from waypoints

To ensure continuity of the path at each WP, one can construct a significantly differentiable path going through the waypoints. The overall desired path $\mathbf{p_d}(s)$ is divided into subpaths between waypoints, expressed as polynomials in s of a chosen order, $p_{d,i}(s)$ with $i = 1, 2, ..., N$. To ensure that each subpath is connected, $\mathbf{p_d}(s) \in \mathcal{C}^r$, the following must be true:

$$\begin{aligned}
\lim_{s \nearrow i-1} x_{d,i-1}(s) &= \lim_{s \searrow i-1} x_{d,i}(s), & \lim_{s \nearrow i-1} y_{d,i-1}(s) &= \lim_{s \searrow i-1} y_{d,i}(s), \\
\lim_{s \nearrow i-1} x^s_{d,i-1}(s) &= \lim_{s \searrow i-1} x^s_{d,i}(s), & \lim_{s \nearrow i-1} y^s_{d,i-1}(s) &= \lim_{s \searrow i-1} y^s_{d,i}(s), \\
&\vdots & &\vdots \\
\lim_{s \nearrow i-1} x^{s^r}_{d,i-1}(s) &= \lim_{s \searrow i-1} x^{s^r}_{d,i}(s), & \lim_{s \nearrow i-1} y^{s^r}_{d,i-1}(s) &= \lim_{s \searrow i-1} y^{s^r}_{d,i}(s),
\end{aligned}$$

for $i \in \mathcal{I} \setminus \{1\}$. Each subpath is given by polynomials of order k,

$$x_{d,i}(s) = a_{k,i}s^k + \ldots + a_{1,i}s + a_{0,i}, \tag{6.3a}$$
$$y_{d,i}(s) = b_{k,i}s^k + \ldots + b_{1,i}s + b_{0,i}, \tag{6.3b}$$

where the coefficients $\{a_{j,i}, b_{j,i}\}$ must be determined by solving a set of linear equations. There are a total of $(k+1) \cdot 2n$ coefficients to find, and this can be done for each subpath independently. To have continuity at the connection points, numerical values that are common for neighboring subpaths is assigned. Skjetne (2005) gives two methods for doing this, direct continuous parametrization, and hybrid parametrization which will be used in this thesis.

6.2.2 Hybrid parametrization of a $\mathcal{C}^r$ path

Each subpath is parametrized within an interval $\theta = s - \lfloor s \rfloor \in [0, 1)$, and identified by an index $i = \lfloor s \rfloor + 1$ indicating subpath number. The operator $\lfloor s \rfloor$ rounds s down to the nearest integer. Then the coefficients for each subpath is calculated independently as a set of linear equations. The equations to calculate the coefficients $\{a_{j,i}, b_{j,i}\}$ is given by

$\mathcal{C}^0$: Continuity at the waypoints for $i \in \mathcal{I}$:

$$\begin{aligned} x_{d,i}(0) &= x_i, & y_{d,i}(0) &= y_i, \\ x_{d,i}(1) &= x_{i+1}, & y_{d,i}(1) &= y_{i+1}. \end{aligned}$$

$\mathcal{C}^1$: The slopes at the first and last waypoints are chosen as:

$$\begin{aligned} x^{\theta}_{d,1}(0) &= x_2 - x_1, & y^{\theta}_{d,1}(0) &= y_2 - y_1, \\ x^{\theta}_{d,n}(1) &= x_{n+1} - x_n, & y^{\theta}_{d,n}(1) &= y_{n+1} - y_n. \end{aligned}$$

The slopes at the intermediate waypoints are given by:

$$\left.\begin{aligned} x^{\theta}_{d,1}(0) &= \lambda(x_{i+1} - x_{i-1}) \\ y^{\theta}_{d,1}(0) &= \lambda(y_{i+1} - y_{i-1}) \end{aligned}\right\} \quad i = 2, ..., n,$$

$$\left.\begin{aligned} x^{\theta}_{d,1}(1) &= \lambda(x_{i+2} - x_i) \\ y^{\theta}_{d,1}(1) &= \lambda(y_{i+2} - y_i) \end{aligned}\right\} \quad i = 1, ..., n-1,$$

where λ is a design constant.

$\mathcal{C}^j$: Setting derivatives of order $j \geq 2$ to zero for $i \in \mathcal{I}$:

$$\begin{aligned} x^{\theta^j}_{d,i}(0) &= 0, & y^{\theta^j}_{d,i}(0) &= 0, \\ x^{\theta^j}_{d,i}(1) &= 0, & y^{\theta^j}_{d,i}(1) &= 0. \end{aligned}$$

Since the path tangential vector is needed to compute the desired heading, the differentiability requirement is $\mathcal{C}^3$. This requires a polynomial of order $k = 7$. The result is the hybrid

parametrization of the path

$$\bar{\mathbf{p}}_d(i,\theta) = \begin{bmatrix} x_{d,i}(\theta) \\ y_{d,i}(\theta) \end{bmatrix}, \tag{6.7}$$

where $i \in \mathcal{I}$ and $\theta \in [0,1)$. We now have the desired $\mathcal{C}^r$ map

$$s \mapsto \mathbf{p}_d(s) := \bar{\mathbf{p}}_{\mathbf{d}}(i(s),\theta(s)), \tag{6.8}$$

which is a continuous parametrization by s (Skjetne; 2005).
Plots with the hybrid path parametrization and the path planning algorithm chosen in section 6.1 with two different λ can be seen Figure 6.3. Note that $\lambda = 0$ gives straight line segments.

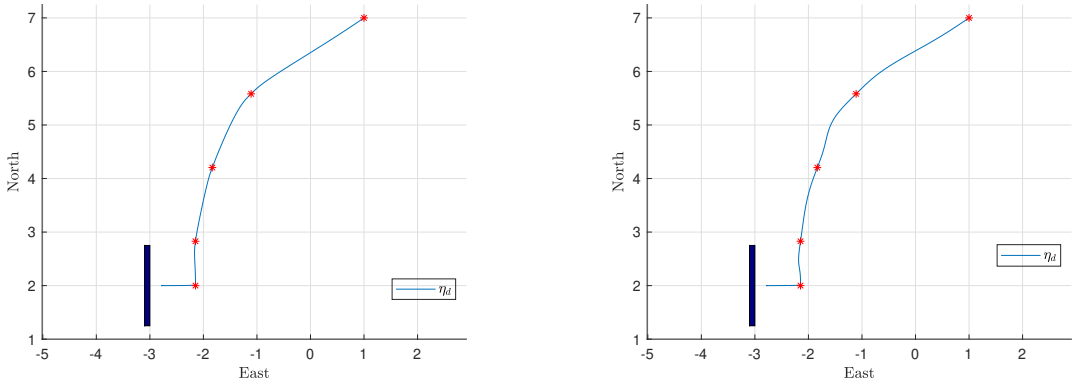

(a) $\lambda = 0.25$. (b) $\lambda = 0.50$.

Figure 6.3: Path generation with different lambda values.

6.3 Guidance laws

Now that the desired path is generated, guidance laws for both phases can be made. Keep in mind that Phase 1 is path following from the inital position p_0, to p_n outside the dock, and Phase 2 is moving the ship towards the dock. Assuming that $\mathbf{p}_{d_1}(s_1)$ denotes a generated path from p_0 to p_n, with derivatives $\mathbf{p}_{d_1}^{s_1} = [x_{d_1}^{s_1}, y_{d_1}^{s_1}]^\top$, and $\mathbf{p}_{d_1}^{s_1^2} = [x_{d_1}^{s_1^2}, y_{d_1}^{s_1^2}]^\top$, Skjetne (2019b) presents theory on the guidance of a vessel during a docking operation with a parametrized path, and will be used here.

6.3.1 Phase 1

Phase 1 consists of setting the vessel up for docking by following the generated path from p_0 to p_n, at a desired speed with a path tangential heading. As s_1 denotes the position along the desired path $\mathbf{p}_{d_1}(s_1)$, $\dot{s}_1$ can be viewed as the speed along the path. The behavior of $\dot{s}_1$ can be manipulated by choosing an appropriate speed assignment, $v_{s_1}(s_1,t)$. This speed

assignment should be designed such that $v_{s_1} > 0$ for $s_1 < N$, $v_{s_1} < 0$ for $s_1 > N$ and $v_{s_1} = 0$ for $s_1 = N$, with N denoting number of path segments. A proposed speed profile v_{s_1}, and its significant derivative $v_{s_1}^{s_1}$ is

$$v_{s_1}(s_1) = \frac{u_d}{|\mathbf{p}_{d_1}^{s_1}(s_1)|} \tanh\left(\frac{N - s_1}{\Delta_u}\right), \tag{6.9}$$

$$v_{s_1}^{s_1} = -\frac{u_d\left(x_{d_1}^{s_1} x_{d_1}^{s_1^2} + y_{d_1}^{s_1} y_{d_1}^{s_1^2}\right)}{\left(x_{d_1}^{s_1\,2} + y_{d_1}^{s_1\,2}\right)^{\frac{3}{2}}} \tanh\left(\frac{N - s_1}{\Delta_u}\right) - \frac{u_d}{\Delta_u\sqrt{x_{d_1}^{s_1\,2} + y_{d_1}^{s_1\,2}}} \operatorname{sech}^2\left(\frac{N - s_1}{\Delta_u}\right), \tag{6.10}$$

with u_d being the desired speed along the path in meters per second. The tanh-component is responsible for giving the ship positive, negative, or zero speed depending on the position of the ship along the path. Δ_u sets the slope as $(N - s_1) \to 0$. When $(N - s_1)$ approaches zero, so does tanh (Figure 6.4). To provide the heading reference during the operation, the tangential vector is required. We have that this, and the normal vector, at any given point along the path, are defined as

$$\mathbf{T}_d(s_1) = \frac{\mathbf{p}_{d_1}^{s_1}(s_1)}{|\mathbf{p}_{d_1}^{s_1}(s_1)|}, \quad \text{and} \quad \mathbf{N}_d(s_1) = \mathbf{J}\mathbf{T}_d(s_1), \tag{6.11}$$

with

$$\mathbf{J} = \begin{bmatrix} 0 & 1 \\ -1 & 0 \end{bmatrix}. \tag{6.12}$$

Setting the desired heading path tangential, this can be found by

$$\psi_{d_1}(s_1) = \angle\mathbf{T}_d(s_1) = \operatorname{atan2}(y_{d_1}^{s_1}(s_1), x_{d_1}^{s_1}(s_1)), \tag{6.13}$$

with derivatives

$$\psi_{d_1}^{s_1}(s_1) = \frac{x_{d_1}^{s_1}(s_1) y_{d_1}^{s_1^2}(s_1) - x_{d_1}^{s_1^2}(s_1) y_{d_1}^{s_1}(s_1)}{x_{d_1}^{s_1}(s_1)^2 + y_{d_1}^{s_1}(s_1)^2}, \tag{6.14}$$

$$\psi_{d_1}^{s_1^2} = \frac{x_{d_1}^{s_1} y_{d_1}^{s_1^3} - x_{d_1}^{s_1^3} y_{d_1}^{s_1}}{x_{d_1}^{s_1\,2} + y_{d_1}^{s_1\,2}} - 2\frac{(x_{d_1}^{s_1} y_{d_1}^{s_1^2} - x_{d_1}^{s_1^2} y_{d_1}^{s_1})(x_{d_1}^{s_1} x_{d_1}^{s_1^2} + y_{d_1}^{s_1} y_{d_1}^{s_1^2})}{(x_{d_1}^{s_1\,2} + y_{d_1}^{s_1\,2})^2}. \tag{6.15}$$

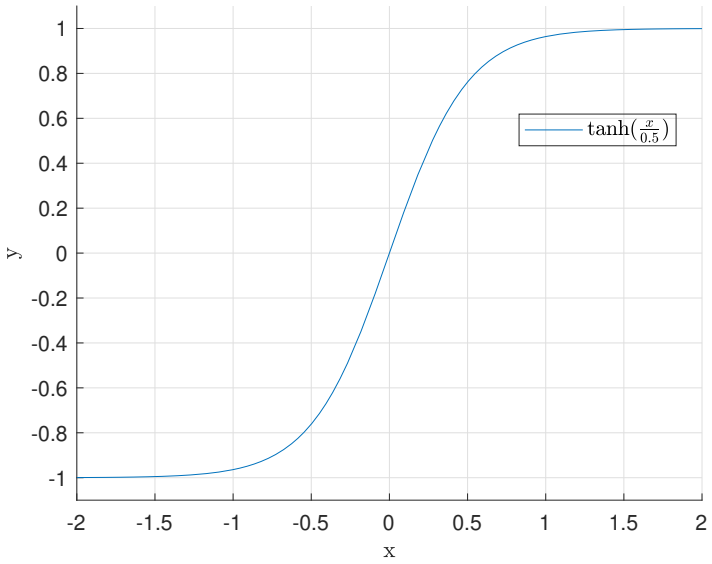

Figure 6.4: Plot of $\tanh\left(\frac{x}{0.5}\right)$.

6.3.2 Phase 2

When reaching the final WP, the proximity sensors will be switched on, providing measurements of the local distance from the shipside to the quayside. These sensors will be used to read the distance to the quay as the ships moves towards it, as well as to calculate the heading correction which needs to be applied when the ship arrives at the last WP to ensure a heading parallel to the quayside. When the heading is parallel, generation of a docking path will start, and the vessel will start moving towards the quay to a set reference distance, d_{ref}.

Heading correction

To calculate the heading correction, the angle of the ship with respect to the dock has to be found. This is computed by utilizing the proximity sensors. From Figure 6.5 we can see that d_1 and d_2 denotes the measurements, $l_1 = x^b_{s_1}$ and $l_2 = x^b_{s_2}$ denotes the position of the sensors along the x-axis in the body frame. The angle between the ship and the quay can then be calculated as

$$\tan(\psi_{corr}) = \frac{d_1 - d_2}{l_1 - l_2} \implies \psi_{corr} = \text{atan2}(\Delta d, \Delta l), \tag{6.16}$$

with $\Delta d = d_1 - d_2$, and $\Delta l = l_1 - l_2$.

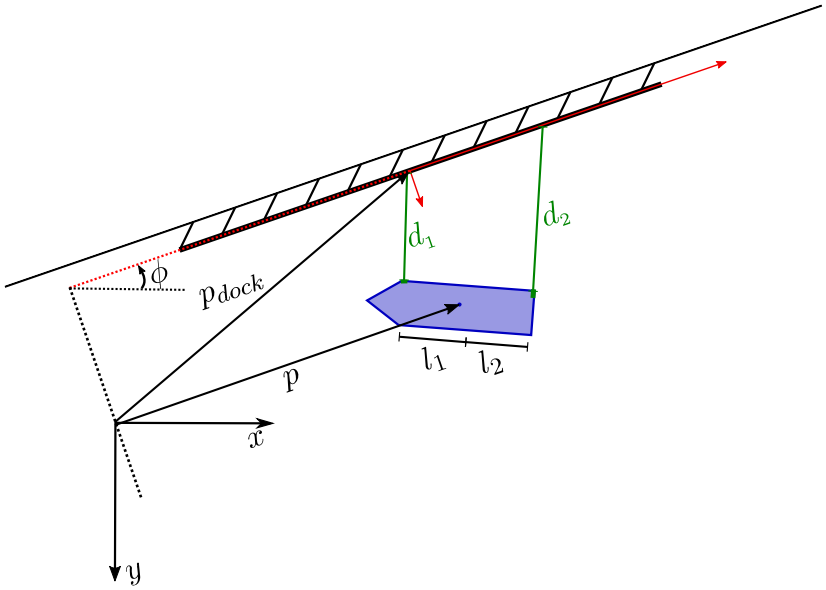

Figure 6.5: Docking operation and sensor measurements.

Docking

When the ship is properly positioned outside the designated docking position with the correct heading, it is time to start moving the ship along the normal vector of the entrance path to p_n, towards the quay. In this approach the sensors will provide information on the distance to the dock to be used in the speed assignment. When the ship has arrived at p_n, a desired docking path is formed along the normal vector, that is parametrized by a new path variable s_2,

$$\mathbf{p_{dock}}(s_1, s_2) = s_2 \mathbf{N}_d(s_1). \tag{6.17}$$

As $\mathbf{N}_d = \mathbf{J}\mathbf{T}_d$ has unit length, s_2 is given in meters out from the path, along $\mathbf{N}_d$. To adjust the behavior along $\mathbf{N}_d$, and to make the vessel come a complete stop at d_{ref}, a speed assignment on $\dot{s_2}$ must be designed based on the proximity sensor measurements. The distance measurement to be compared to d_{ref} is chosen to be

$$d(t) = \min\{d_1, d_2\}. \tag{6.18}$$

One could also choose to use the mean of the two sensor measurements, but Equation 6.18 is chosen to avoid colliding with the dock if the heading is to become non-parallel to the dock during the operation. Letting the difference $d - d_{ref}$ be denoted as $\tilde{d}$, a proposed speed assignment for $\dot{s}_2$ is

$$\dot{s}_2 = v_{s_2} = u_{dock} \tanh\left(\frac{\tilde{d}}{\Delta_p}\right), \tag{6.19}$$

with u_{dock} being the desired docking speed, Δ_p is a gain to decide the slope of tanh as $\tilde{d} \to 0$. Similar to the speed assignment in Phase 1, tanh ensures a positive speed for $\tilde{d} > 0$, negative for $\tilde{d} < 0$, and zero for $\tilde{d} = 0$. This results in uniform global asymptotic stability for s_2 at a position $\tilde{d} = 0$, as proved by Skjetne (2019b).

6.3.3 Combined guidance system

The guidance laws for phases 1 and 2 are combined by using activation functions in the transition between phases to activate the proper terms. The following is a proposed guidance system for the whole autonomous docking operation:

$$\dot{s}_1 = v_{s_1} + \omega = \frac{u_d}{|\mathbf{p}_{d_1}(s_1)|} \tanh\left(\frac{N - s_1}{\Delta_u}\right) + \omega, \tag{6.20a}$$

$$\dot{s}_2 = \sigma_{dock} v_{s_2} = \sigma_{dock} u_{dock} \tanh\left(\frac{\tilde{d}}{\Delta_p}\right), \tag{6.20b}$$

$$\begin{aligned} \psi_d &= \psi_{d_1}(s_1) + \sigma_\psi \psi_{corr}, \\ &= \text{atan2}(y^s_{d_1}(s_1), x^s_{d_1}(s_1)) + \sigma_\psi \text{atan2}(\Delta d, \Delta l), \end{aligned} \tag{6.20c}$$

$$\begin{aligned} \mathbf{p}_d &= \mathbf{p}_{d_1}(s_1) + \mathbf{p}_{dock}(s_1, s_2) \\ &= \mathbf{p}_{d_1}(s_1) + s_2 \mathbf{N}_d(s_1), \end{aligned} \tag{6.20d}$$

with

$$\sigma_\psi = \begin{cases} 1, & \text{if} \quad s_1 = N + \epsilon_{ph1} \\ & \text{and } \dot{s}_1 = 0 \\ 0, & \text{else} \end{cases}, \qquad \sigma_{dock} = \begin{cases} 1, & \text{if} \quad \sigma_\psi = 1 \\ & \text{and } \text{atan2}(\Delta d, \Delta l) < \epsilon_\psi \\ 0, & \text{else} \end{cases} \tag{6.21}$$

being activation functions that either have the value 0 or 1, to respectively deactivate or activate the term associated with it. σ_ψ is activated when the vessel arrives at p_n inside an accepted error ϵ_{ph1}, and $\dot{s}_1 = 0$, activating the heading correction term in ψ_d. σ_{dock} is activated when $\sigma_\psi = 1$ and the heading is parallel to the dock within a certain error ϵ_ψ, activating $\dot{s_2}$ which starts generating a docking path for the ship to follow towards the dock. ω is a maneuvering update law which will be decided in the motion controller.

6.3.4 Situational reactiveness based on proximity sensor measurements

Simple situational awareness and reactiveness can be implemented using the proximity sensor measurements. As these sensors only provide information on the surroundings with a small field of view in one direction, the complexity of the situational awareness provided is limited.

Detection of drop in measurements

As the sensors only provide information in the form of distance from the sensor to an object reflecting the signal in the field of view, this measurement must be analyzed to detect eventual obstacles in the docking path. One way of doing this is to analyze the sensors measurements for drops. During docking, the distance measurement to the quay side should be continuously decreasing as a function of speed in sway. If something was to enter a sensor's field of view, this would result in a sudden drop in the distance measured by the sensor. The described situation is illustrated in Figure 6.6, with the accompanying measurement reading of proximity sensor 2 in Figure 6.7.

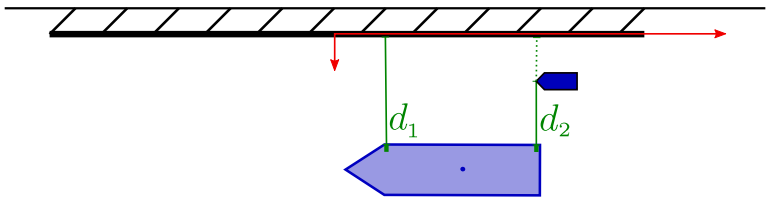

Figure 6.6: Illustration of obstacle entering the field of view of proximity sensor 2.

By checking the sensor measurements for drops of the like as the one in Figure 6.7, one could choose a preferred reaction to such a situation in the guidance system. Letting $d_i(k)$ denote the sensor reading for sensor i at sampling time k, drop detection can be easily implemented by checking if $d_i(k-1) - d_i(k) > \epsilon_1$ with ϵ_1 being a threshold for the detected drop to be considered a danger or not. Typically ϵ_1 should be chosen to be larger than the expected fluctuations between each measurement reading, but not so large that a significant drop is not detected.

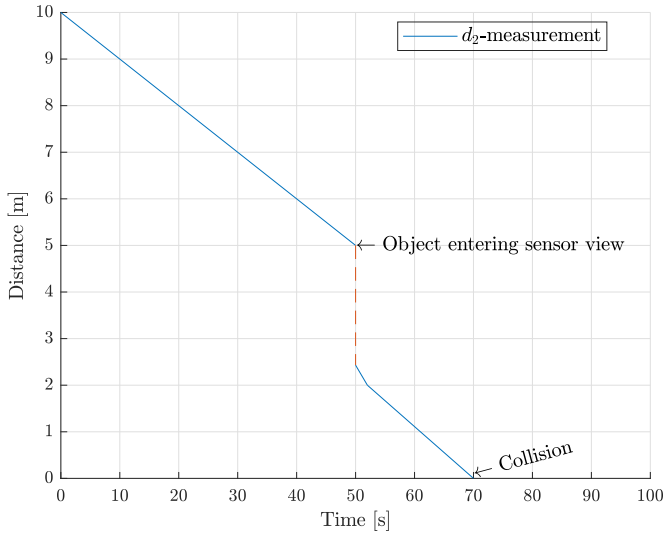

Figure 6.7: d_2 measurement as a function of time. The vessel is moving towards the dock with a constant speed. An obstacle enters the field of view at 50 seconds, and remains there for the rest of the simulation. The ship continues towards the dock, and collides with the obstacle at 70 seconds.

Another method of drop detection could be to compare $d_i(k-1) - d_i(k) = \Delta_d$ to the mean difference in sensor measurement over a chosen interval of samplings before measurement k, $\frac{1}{c}\sum_{n=1}^{c} d_i(k-n-1) - d_i(k-n) = \bar{\Delta}_{d_c}$, with c being the number of measurements considered when calculating the mean difference. If $\Delta_d - \bar{\Delta}_{d_c} > \epsilon_2$, danger could be considered detected, with ϵ_2 being a chosen threshold for detection of danger. This method, called the moving average, might be preferred as it accounts for fluctuations in the measurements, such as unfiltered noise or other fluctuations.

Reaction to danger

If a significant drop is detected in the measurements a response must be chosen. A reaction could be to stop the vessel and freeze s_2, enabling dynamic positioning by setting $u_{dock} = 0 \implies \dot{s}_2 = 0$. The situational reactiveness system logic for this reaction is visualized in Figure 6.8.

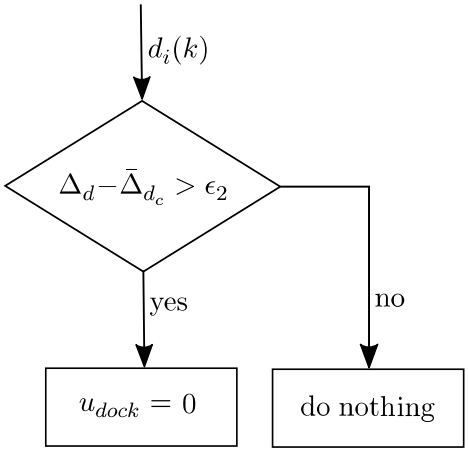

Figure 6.8: Flowchart of a situational reactiveness system.

Another reaction could be to move the ship back to the position it had when initiating Phase 2, at $s_2 = 0$. To do this, one could set $u_{dock} = -u_{dock}$, making the vessel motion go the opposite way. To make sure the vessel stops when arriving at $s_2 = 0$ a tanh-function is added. The resulting situational reactiveness system can be written as

$$u_{dock} = \begin{cases} -u_{dock} \tanh\left(\frac{s_2}{\Delta_{s2}}\right) & \text{if danger detected} \\ u_{dock} & \text{else} \end{cases}, \tag{6.22}$$

where Δ_{s2} is a gain deciding the slope of tanh as s_2 goes towards 0.

Chapter 7

Control system

The control system is responsible for utilizing the ship actuators to follow the given set points from the guidance system, by calculating generalized and individual thruster forces. This system consists of two main components:

- The motion controller which calculates generalized desired forces from the current and desired ship position and orientation, $\boldsymbol{\eta}$ and $\boldsymbol{\eta_d}$.
- The control allocation which calculates the individual thruster set points given the desired generalized forces.

7.1 Motion controller

The controller of choice will be an uncoupled cascaded backstepping controller presented in Skjetne (2020), and is based on the 3 DOF control design model. In this cascaded backstepping design, individual controls for the two subsystems are designed, which implies that the CLF from step 1, $\mathbf{V_1}$, will not be included in the CLF for step 2, $\mathbf{V_2}$. Skjetne (2020) starts with step 2, assuming $\boldsymbol{\alpha}$ and $\dot{\boldsymbol{\alpha}}$ are given, while actually designing $\boldsymbol{\alpha}$ after. Letting $\mathbf{s} := [s_1, s_2]^\top \in \mathbb{R}^2$. We have a parametrized path $\mathbf{p}_d : \mathbb{R}^2 \to \mathbb{R}^2$ and heading reference $\psi_d : \mathbb{R}_{\geq 0} \times \mathbb{R}^2 \to \mathbb{S}^1$. This gives the desired output pose

$$\boldsymbol{\eta_d}(t, \mathbf{s}) := \begin{bmatrix} \mathbf{p}_d(s_1, s_2) \\ \psi_d(t, s_1, s_2) \end{bmatrix}. \tag{7.1}$$

We also assume a desired speed assignment for $\mathbf{s}$, given by $v : \mathbb{R}_{\geq 0} \times \mathbb{R}^2 \to \mathbb{R}^2$, given by

$$\boldsymbol{v}(t, \mathbf{s}) := \begin{bmatrix} v_1(t, s_1, s_2) \\ v_2(t, s_1, s_2) \end{bmatrix}. \tag{7.2}$$

Assuming that $\mathbf{p}_d$ is designed such that $\mathbf{s} \to \mathbf{p}_d(\mathbf{s})$ spans $\mathbb{R}^2$, we do the cascaded backstepping design by starting with Step 2.

Step 2:
Assuming that the virtual control $\boldsymbol{\alpha}(t, s, \eta)$ and its derivative $\dot{\boldsymbol{\alpha}}$ are available, with $\mathbf{s}$ being the path parametrization vector and $\boldsymbol{\upsilon}(t, s)$ the speed assignment for $\dot{\mathbf{s}}$.

Defining

$$\mathbf{z_2} := \boldsymbol{\nu} - \boldsymbol{\alpha}(s, t, \eta). \tag{7.3}$$

The objective is to control Equation 7.3 exponentially to zero. Differentiating Equation 7.3 yields

$$\mathbf{M}\dot{\mathbf{z}}_2 = \mathbf{M}\dot{\boldsymbol{\nu}} - \mathbf{M}\dot{\boldsymbol{\alpha}} = -\mathbf{D}\boldsymbol{\nu} + \boldsymbol{\tau} + \mathbf{b} - \mathbf{M}\dot{\boldsymbol{\alpha}}. \tag{7.4}$$

Defining a control Lyapunov function for step 2, $\mathbf{V_2}$, to be

$$\mathbf{V_2} = \frac{1}{2}\mathbf{z_2}^\top \mathbf{M}\mathbf{z_2}, \tag{7.5}$$

differentiating $\mathbf{V_2}$ yields

$$\begin{aligned} \dot{\mathbf{V}}_\mathbf{2} &= \mathbf{z_2}^\top \mathbf{M}\dot{\mathbf{z}}_\mathbf{2} && (7.6)\\ &= \mathbf{z_2}^\top \left(-\mathbf{D}\boldsymbol{\nu} + \boldsymbol{\tau} + \mathbf{b} - \mathbf{M}\dot{\boldsymbol{\alpha}}\right). && (7.7)\\ & && (7.8) \end{aligned}$$

Assigning the control law

$$\boldsymbol{\tau} = -\mathbf{K_2}\mathbf{z_2} + \mathbf{D}\boldsymbol{\alpha} - \hat{\mathbf{b}} + \mathbf{M}\dot{\boldsymbol{\alpha}}, \qquad \mathbf{K_2} = \mathbf{K_2}^\top \succ 0. \tag{7.9}$$

Assuming that $\hat{\mathbf{b}} \approx \mathbf{b}$ is an estimate of the bias given by the observer, this is used to directly compensate for $\mathbf{b}$. This yields

$$\dot{\mathbf{V}}_\mathbf{2} = -\mathbf{z_2}^\top(\mathbf{K_2} + \mathbf{D})\mathbf{z_2} \leq 0, \tag{7.10}$$

and

$$\mathbf{M}\dot{\mathbf{z}}_\mathbf{2} = -(\mathbf{K_2} + \mathbf{D})\mathbf{z_2}. \tag{7.11}$$

$\mathbf{z_2} = 0$ is then UGES for the $\dot{\mathbf{z}}_\mathbf{2}$-subsystem, since $(\mathbf{K_2} + \mathbf{D}) > 0$.

Letting $\mathbf{T_2} = \text{diag}(T_u, T_v, T_r)$ be a diagonal matrix of time constants for the $\mathbf{z_2}$-subsystem,

and setting $\mathbf{K_2} = \mathbf{M}{\mathbf{T_2}}^{-1} - \mathbf{D}$ yields

$$\dot{\mathbf{z}}_\mathbf{2} = -{\mathbf{T_2}}^{-1}\mathbf{z_2}. \tag{7.12}$$

With this concluding Step 2, $\boldsymbol{\alpha}$ must now be designed in step 1 such that it exponentially stabilizes the $\dot{\mathbf{z}}_\mathbf{1}$-subsystem with $\mathbf{z_2}$ entering through a linear interconnection function.

Step 1:
Assume that the desired path map $\boldsymbol{\eta_d} : \mathbb{R}^2 \to \mathbb{R}^2 \times \mathcal{S}$ and the continuous path parameter $\mathbf{s} \in \mathbb{R}^2$ are available, and $\upsilon_i(t, s_i)$ a speed assignment for $\dot{s}_i$, with $i = 1, 2$. Also assume the 3 DOF body fixed linear and angular velocities $\boldsymbol{\nu} = [u, v, r]^\top$ available, with $\boldsymbol{\nu_p} = [u, v]^\top$. The control for the position and heading will be decoupled and then combined into the virtual control $\boldsymbol{\alpha}$ in the end.

Defining the error variables

$$\mathbf{z_{1,p}} := \mathbf{R_2}(\psi)^\top[\mathbf{p} - \mathbf{p}_d(s_1, s_2)], \quad z_{1,\psi} := \psi - \psi_d(t, s_1, s_2), \quad \mathbf{z_1} := [{\mathbf{z_{1,p}}}^\top, z_{1,\psi}]^\top, \tag{7.13}$$

$$\mathbf{z_{2,p}} := \boldsymbol{\nu_p} - \boldsymbol{\alpha_p}, \quad z_{2,\psi} := r - \alpha_\psi, \quad \mathbf{z_2} := [{\mathbf{z_{2,p}}}^\top, z_{2,\psi}]^\top, \quad \boldsymbol{\alpha} := [{\boldsymbol{\alpha_p}}^\top, \alpha_\psi]^\top, \tag{7.14}$$

$$\omega_1 := \dot{s}_1 - \upsilon_1(t, s_1, s_2), \quad \omega_2 := \dot{s}_2 - \upsilon_2(t, s_1, s_2), \tag{7.15}$$

$$\boldsymbol{\upsilon} := [\upsilon_1, \upsilon_2]^\top, \quad \boldsymbol{\omega} := [\omega_1, \omega_2]^\top = \dot{\mathbf{s}} - \boldsymbol{\upsilon}(t, s). \tag{7.16}$$

The design for the position and heading will be individually designed, as follows.
A maneuvering design is done for the position:

$$\dot{\mathbf{z}}_\mathbf{1,p} = \dot{\mathbf{R}}_2(\psi)^\top[\mathbf{p} - \mathbf{p}_d(s_1, s_2)] + \mathbf{R_2}(\psi)^\top[\dot{\mathbf{p}} - \mathbf{p}_d^{s_1}(s_1, s_2)\dot{s}_1 - \mathbf{p}_d^{s_2}(s_1, s_2)\dot{s}_2], \tag{7.17}$$

$$= -\mathbf{S_2}(r)\mathbf{z_{1,p}} + \mathbf{z_{2,p}} + \boldsymbol{\alpha_p} - \mathbf{R_2}(\psi)^\top\mathbf{p}_d^{s_1}(\omega_1 + \upsilon_1) - \mathbf{R_2}(\psi)^\top\mathbf{p}_d^{s_2}(\omega_2 + \upsilon_2). \tag{7.18}$$

Choosing the first control Lyapunov function,

$$\mathbf{V_{1,p}} = \frac{1}{2}{\mathbf{z_{1,p}}}^\top\mathbf{z_{1,p}}, \tag{7.19}$$

$$\dot{\mathbf{V}}_\mathbf{1,p} = {\mathbf{z_{1,p}}}^\top\left[-\mathbf{S_2}(r)\mathbf{z_{1,p}} + \mathbf{z_{2,p}} + \boldsymbol{\alpha_p} - \mathbf{R_2}(\psi)^\top\mathbf{p}_d^{s_1}(\omega_1 + \upsilon_1) - \mathbf{R_2}(\psi)^\top\mathbf{p}_d^{s_2}(\omega_2 + \upsilon_2)\right], \tag{7.20}$$

and the virtual $\mathbf{p}$-control,

$$\boldsymbol{\alpha_p} = -\mathbf{K_{1,p}}\mathbf{z_{1,p}} + \mathbf{R_2}(\psi)^\top\mathbf{p}_d^{s_1}\upsilon_1 + \mathbf{R_2}(\psi)^\top\mathbf{p}_d^{s_2}\upsilon_2, \quad \mathbf{K_{1,p}} = {\mathbf{K_{1,p}}}^\top \succ 0, \tag{7.21}$$

as well as the tuning functions with respect to s_1 and s_2

$$\rho_1 = -\mathbf{z_{1,p}}^\top \mathbf{R_2}(\psi)^\top \mathbf{p}_d^{s_1} = V_{1,p}^{s_1}(s_1, s_2, \mathbf{p}, \psi), \tag{7.22}$$
$$\rho_2 = -\mathbf{z_{1,p}}^\top \mathbf{R_2}(\psi)^\top \mathbf{p}_d^{s_2} = V_{1,p}^{s_2}(s_1, s_2, \mathbf{p}, \psi), \tag{7.23}$$

results in

$$\dot{V}_{1,p} = -\mathbf{z_{1,p}}^\top \mathbf{K_{1,p}} \mathbf{z_{1,p}} + \mathbf{z_{1,p}}^\top \mathbf{z_{2,p}} + \rho_1 \omega_1 + \rho_2 \omega_2, \tag{7.24}$$
$$\dot{\mathbf{z}}_{\mathbf{1,p}} = -(\mathbf{S_2}(r) + \mathbf{K_{1,p}})\mathbf{z_{1,p}} + \mathbf{z_{2,p}} - \mathbf{R_2}(\psi)^\top \left(\mathbf{p}_d^{s_1}\omega_1 + \mathbf{p}_d^{s_2}\omega_2\right), \tag{7.25}$$

where $\mathbf{z_{2,p}} = \begin{bmatrix}\mathbf{I}_{2\times 2} & \mathbf{0}_{2\times 1}\end{bmatrix} \mathbf{z_2}$, and $\mathbf{S_2}(r) = \begin{bmatrix}0 & -r \\ r & 0\end{bmatrix}$.

Assuming $\dot{\psi}_d$ is available, a direct tracking design is done for the heading:

$$\dot{z}_{1,\psi} = \dot{\psi} - \dot{\psi}_d = z_{2,\psi} + \alpha_\psi - \dot{\psi}_d, \tag{7.26}$$
$$V_{1,\psi} = \frac{1}{2} z_{1,\psi}^2, \tag{7.27}$$
$$\dot{V}_{1,\psi} = z_{1,\psi}\left[z_{2,\psi} + \alpha_\psi - \dot{\psi}_d\right], \tag{7.28}$$
$$\alpha_\psi = -k_{1,\psi} z_{1,\psi} + \dot{\psi}_d, \quad k_{1,\psi} > 0, \tag{7.29}$$
$$\dot{V}_{1,\psi} = -k_{1,\psi} z_{1,\psi}^2 + z_{1,\psi} z_{2,\psi}, \tag{7.30}$$
$$\dot{z}_{1,\psi} = -k_{1,\psi} z_{1,\psi} + z_{2,\psi}, \tag{7.31}$$

where $z_{2,\psi} = \begin{bmatrix}\mathbf{0}_{1\times 2} & 1\end{bmatrix} \mathbf{z_2}$.

Let $\mathbf{T_{1,p}} = \mathrm{diag}(T_x, T_y)$ be a diagonal matrix of time constants for the $\mathbf{z_{1,p}}$-subsystem and T_ψ a time constant for the $z_{1,\psi}$-subsystem, set $\mathbf{K_{1,p}} = \mathbf{T_{1,p}}^{-1}$ and $k_{1,\psi} = 1/T_\psi$, and assume $\mathbf{S_2}(r)\mathbf{z_{1,p}} + \mathbf{R_2}(\psi)^\top(\mathbf{p}_d^{s_1}\omega_1 + \mathbf{p}_d^{s_2}\omega_2) = 0$. Then the simplified system

$$\mathbf{T_{1,p}}\dot{\mathbf{z}}_{\mathbf{1,p}} = -\mathbf{z_{1,p}} + \mathbf{T_{1,p}}\mathbf{z_{2,p}}, \tag{7.32}$$
$$T_\psi \dot{z}_{1,\psi} = -z_{1,\psi} + T_\psi z_{2,\psi}, \tag{7.33}$$
$$\mathbf{T_2}\dot{\mathbf{z}}_\mathbf{2} = -\mathbf{z_2}, \tag{7.34}$$

is used for tuning $\mathbf{T_{1,p}}$, $T_{1,\psi}$ and $\mathbf{T_2}$, which again determines the gains $\mathbf{K_{1,p}}$, $K_{1,\psi}$ and $\mathbf{K_2}$. It is recommended to set $\mathbf{T_2} < \mathrm{diag}(\mathbf{T_{1,p}}, T_{1,\psi})$ to make the $\mathbf{z_2}$-subsystem faster than $\mathbf{z_1}$.

When doing Step 2, both $\boldsymbol{\alpha}$ and $\dot{\boldsymbol{\alpha}}$ was required. Differentiating $\boldsymbol{\alpha}$ gives

$$\begin{aligned}\dot{\boldsymbol{\alpha}}_{\boldsymbol{p}} &= \mathbf{K_{1,p}}\mathbf{S_2}(r)\mathbf{z_{1,p}} - \mathbf{K_{1,p}}\boldsymbol{\upsilon} + \mathbf{K_{1,p}}\mathbf{R_2}(\psi)^\top \left(\mathbf{p}_d^{s_1}\dot{s_1} + \mathbf{p}_d^{s_2}\dot{s_2}\right) \\ &\quad - \mathbf{S_2}(r)\mathbf{R_2}(\psi)^\top \left(\mathbf{p}_d^{s_1}\upsilon_1 + \mathbf{p}_d^{s_2}\upsilon_2\right) \\ &\quad + \mathbf{R_2}(\psi)^\top \left(\mathbf{p}_d^{s_1^2}\upsilon_1\dot{s}_1 + \mathbf{p}_d^{s_1}\upsilon_1^{s_1}\dot{s}_1 + \mathbf{p}_d^{s_1}\upsilon_1^{s_2}\dot{s}_2 + \mathbf{p}_d^{s_1}\upsilon_1^t\right) \\ &\quad + \mathbf{R_2}(\psi)^\top \left(\mathbf{p}_d^{s_2^2}\upsilon_2\dot{s}_2 + \mathbf{p}_d^{s_2}\upsilon_2^{s_1}\dot{s}_1 + \mathbf{p}_d^{s_2}\upsilon_2^{s_2}\dot{s}_2 + \mathbf{p}_d^{s_2}\upsilon_2^t\right), \end{aligned} \tag{7.35}$$

$$\dot{\alpha}_\psi = -k_{1,\psi}\left(r - \dot{\psi}_d\right) + \ddot{\psi}_d \tag{7.36}$$

It is now time to decide the maneuvering update laws, to make them act only in the output space of $\mathbf{p}$. Wanting to render

$$\dot{V}_{1,p}\Big|_{z_{2,p}=0} = -\mathbf{z_{1,p}}^\top \mathbf{K_{1,p}}\mathbf{z_{1,p}} + \rho_1\omega_1 + \rho_2\omega_2 \tag{7.37}$$

negative definite in $\mathbf{z_{1,p}}$, we choose ω_1 and ω_2 and implement these in

$$\dot{\mathbf{s}} = \boldsymbol{\upsilon}(t,s) + \boldsymbol{\omega}\begin{cases}\dot{s}_1 = v_1(t,s_1,s_2) + \omega_1 \\ \dot{s}_2 = v_2(t,s_1,s_2) + \omega_2.\end{cases} \tag{7.38}$$

By choosing the unit-tangent gradient update law, we get

$$\omega_1 = \frac{-\mu_1\rho_1}{|\mathbf{p}_d^{s_1}(s_1,s_2)| + \epsilon} = \mu_1\frac{\mathbf{p}_d^{s_1}(s_1,s_2)^\top}{|\mathbf{p}_d^{s_1}(s_1,s_2)| + \epsilon}\mathbf{R_2}(\psi)\mathbf{z_{1,p}}, \quad \mu_1 \geq 0 \tag{7.39}$$

$$\omega_2 = \frac{-\mu_2\rho_2}{|\mathbf{p}_d^{s_2}(s_1,s_2)| + \epsilon} = \mu_2\frac{\mathbf{p}_d^{s_2}(s_1,s_2)^\top}{|\mathbf{p}_d^{s_2}(s_1,s_2)| + \epsilon}\mathbf{R_2}(\psi)\mathbf{z_{1,p}}, \quad \mu_2 \geq 0 \tag{7.40}$$

where $0 < \epsilon \ll 1$ is a small constant. Both of these give $\rho_1\omega_1 \leq 0$ and $\rho_2\omega_2 \leq 0$.

Update laws with respect to docking

Assuming we have a path $\mathbf{p}_d(s_1,s_2) = \mathbf{p}_{d_1}(s_1) + s_2\mathbf{N_{d_1}}(s_1)$, where $\mathbf{p}_{d_1}$ is a straight-line path. We then get that $\mathbf{T_d^{s_1}} = \mathbf{N_d^{s_1}} = 0$. This yields

$$V_{1,p}^{s_1} = \rho_1 = -\mathbf{z_{1,p}}^\top \mathbf{R_2}(\psi)^\top \mathbf{p}_d^{s_1} = -(\mathbf{p} - \mathbf{p}_d)^\top \mathbf{T_d^{s_1}}|\mathbf{p}_{d_1}^{s_1}|, \tag{7.41a}$$

$$V_{1,p}^{s_2} = \rho_2 = -\mathbf{z_{1,p}}^\top \mathbf{R_2}(\psi)^\top \mathbf{p}_d^{s_2} = -(\mathbf{p} - \mathbf{p}_d)^\top \mathbf{N_d}. \tag{7.41b}$$

This implies that $V_{1,p}^{s_1} = 0$ when $(\mathbf{p} - \mathbf{p}_d)$ and $\mathbf{T_d^{s_1}}$ are perpendicular, and that $V_{1,p}^{s_2} = 0$ when $(\mathbf{p} - \mathbf{p}_d) = 0$. From this it can be seen that $\mu_1 \gg 0$ will make s_1 jump to the value where $\mathbf{p}$ is projected onto the path $\mathbf{p}_{d_1}$, and $\mu_2 \gg 0$ will make s_2 jump to the value where $\mathbf{p}_d = \mathbf{p}$. Since the vessel is to dock in a safe manner, calm and controlled behavior is desired, therefore a jump in s_2 may be undesired. To avoid this and make the transversal motion pure tracking behavior, $\mu_2 = 0$ is advised. When Phase 2 is commencing, and the

docking starts, $\mu_1 = 0$ is advised so that the position along $\mathbf{p}_{d_1}$ stays firmly at the point where Phase 1 ended.

7.2 Control allocation

The thruster allocation is a vital part of the control system, as it calculates the individual thruster input from the generalized desired forces. The rectangular thruster allocation found in Fossen (2011) will be used. Having the thrust mapping given by

$$\boldsymbol{\tau} = \mathbf{B}\mathbf{f}, \tag{7.42}$$

with $\mathbf{f}$ being a column vector consisting of elements representing the thrust in x^b- and y^b-direction for each thruster. For example, a fixed tunnel thruster will only contribute with one element as it can only give thrust in one direction. An Azimuth thruster contributes with two elements according to the superposition principle, one for thrust in x^b-direction, and one for thrust in y^b-direction. $\mathbf{B}$ is the extended thrust configuration matrix where the rows give how the forces from each thruster in each direction contribute to the three DOFs, and the columns represent the actuators. Several methods exists for determining $\mathbf{f}$, but the widely used weighted Moore-Penrose pseudoinverse from Skjetne (2019a) is used here,

$$\mathbf{f} = \mathbf{B}^{\dagger}\boldsymbol{\tau}, \qquad \mathbf{B}^{\dagger} = \mathbf{B}^{\top}(\mathbf{B}\mathbf{B}^{\top})^{-1}. \tag{7.43}$$

It is important to keep in mind that this solution does not take into account constraints like thruster saturation and forbidden sectors. When $\mathbf{f}$ is calculated, the total commanded force for each thruster, $f_{cmd,i}$, can be calculated. For an Azimuth thruster this is calculated as

$$f_{cmd,i} = \sqrt{f_{i,x}^2 + f_{i,y}^2}, \tag{7.44}$$

with angle

$$\alpha_i = \text{atan2}(f_{i,y}, f_{i,x}), \tag{7.45}$$

where $f_{i,x}$ and $f_{i,y}$ is the desired force in the two directions for thruster i, given in $\mathbf{f}$.
For a tunnel thruster, the commanded force is simply

$$f_{cmd,i} = f_i. \tag{7.46}$$

The normalized desired thruster input for each thruster is then calculated as

$$u_i = \frac{f_{cmd,i}}{k_i}, \tag{7.47}$$

with k_i being a gain scaling the thrust of each thruster.

Chapter 8

Simulation setup

This chapter will present the model ship used in the simulation cases, how the simulations were conducted, and the preparatory work on CSEI in the laboratory and.

8.1 CyberShip Enterprise I

The model ship to be used for this thesis is the CyberShip Enterprise I (CSEI), which is a 1:50 scale model of a tug boat, NTNU (2020). The ship is fitted with two Voith Schneider propellers (VSP) astern, and one bow thruster (BT). CSEI is shown in Figure 8.1 with corresponding measurements in Table 8.2. It is used mostly for dynamic positioning, maneuvering systems testing, and path following experiments. The parameters used in the $\mathbf{M}-, \mathbf{C}-$ and $\mathbf{D}-$matrices in the simulation model and control design model are found in NTNU (2020), and are presented in Table 8.3. To keep the simulations close to real world experiments on CSEI, simple thruster dynamics will be implemented on the simulation model.

Table 8.1: CSEI main data

Parameter	Symbol	Value
Length over all	L_{oa}	1.105 m
Beam	B	0.284 m
Mass	m	14.11 kg

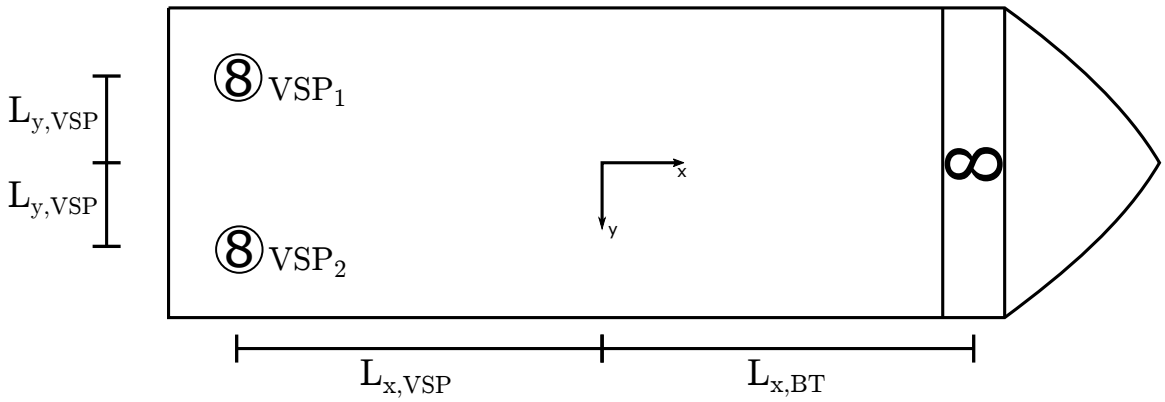

Figure 8.1: Technical drawing of CSEI

Table 8.2: Actuator positions of CSEI

Parameter	Symbol	Value [m]
x length to VSP	$L_{x,VSP}$	0.4574
x length to BT	$L_{x,BT}$	0.3875
y length to VSP	$L_{y,VSP}$	0.055

Table 8.3: CSEI rigid body, added mass and damping coefficients. Courtesy of NTNU (2020).

Rigid body		Added mass		Damping	
Parameter	Value	Parameter	Value	Parameter	Value
m	14.11	$X_{\dot{u}}$	-2	X_u	-0.6555
I_z	1.76	$Y_{\dot{v}}$	-10	Y_v	-1.33
x_g	0.0375	$Y_{\dot{r}}$	0	Y_r	-7.25
y_g	0	$N_{\dot{r}}$	-1	N_v	0.0
-	-	-	-	N_r	-1.9

8.2 Preparatory work on CSEI

As a part of preparing for experiments, the servos on CSEI had to be tuned, as these were not working satisfactorily. Also, thruster measurements and an update of the thruster mapping needed to be done for the ship to work, as these has changed over time.

The servos controlling the two VSPs was tuned to properly give thrust in the desired direction according to the input from thruster allocation. After the servos were tuned,

several bollard pull tests was done to map the thrust given from each thruster for different control inputs. This work culminated in a 2020 update of NTNU (2020), which now includes detailed guides on how to tune the servos and how to undertake the thruster input to force mapping, including the bollard pull test.

The newly found thruster data will be used in the simulations of this thesis, to implement the correct thruster dynamics.

8.3 Implementation of thruster allocation and dynamics of CSEI

To calculate the individual thruster inputs on CSEI, the method in section 7.2 will be implemented. The extended thrust configuration matrix $\mathbf{B}$ to be used in Equation 7.43 is given as

$$\mathbf{B} = \begin{bmatrix} 1 & 0 & 1 & 0 & 0 \\ 0 & 1 & 0 & 1 & 1 \\ L_{y,VSP} & -L_{x,VSP} & -L_{y,VSP} & -L_{x,VSP} & L_{x,BT} \end{bmatrix}, \tag{8.1}$$

which will result in a $\mathbf{f}$-matrix on the form

$$\mathbf{f} = \begin{bmatrix} f_{VSP1,x} & f_{VSP1,y} & f_{VSP2,x} & f_{VSP2,y} & f_{BT} \end{bmatrix}^\top. \tag{8.2}$$

A simple thruster dynamics block is made using the results from the laboratory experiments on the vessel. The thruster input vector $\mathbf{u}$ and VSP angles $\boldsymbol{\alpha}$ are used to calculate the resulting received forces from the thrusters. The input to thruster forces mappings can be approximated as linear functions, as described in NTNU (2020). The yielded thruster forces and moments are calculated as shown below.

For the VSPs:

$$\tau_x = u f_{max} \cos(\alpha), \tag{8.3a}$$
$$\tau_y = u f_{max} \sin(\alpha), \tag{8.3b}$$
$$\tau_n = \tau_x L_{y,VSP} - \tau_y L_{x,VSP}, \qquad (VSP_1) \tag{8.3c}$$
$$\tau_n = -\tau_x L_{y,VSP} - \tau_y L_{x,VSP}, \qquad (VSP_2) \tag{8.3d}$$

For the bow thruster:

$$\tau_x = 0, \tag{8.3e}$$
$$\tau_y = u f_{max}, \tag{8.3f}$$
$$\tau_n = \tau_y L_{x,BT}. \tag{8.3g}$$

This simple thruster dynamic does not account for constraints like forbidden thruster zones, thruster losses due to forward speed, hydrodynamic phenomena, or limits in turn rate.

Chapter 9

Results

In this chapter the results from the simulations testing the ADC will be presented and discussed.

9.1 Simulations

First the observer will be verified, then autonomous docking will be simulated. Several scenarios will be simulated showing regular operation. Lastly, an autonomous docking case with an obstacle entering the docking path will be simulated to demonstrate the situational awareness and reactiveness. Measurements in the simulation will be polluted with zero-mean Gaussian white measurement noise of power 10^{-6}. A constant current, $\boldsymbol{\nu}_c$, with velocity 0.01 m/s going southeast is present in all simulations. The parameters used in the navigation, guidance, and control systems that make up the ADC is presented in Table 9.1.

Links to informative animations showing the operations can be found in Appendix B. These might give a better impression of the operations undertaken than just the plots alone.

Table 9.1: ADC simulation parameters.

Navigation		Guidance		Control	
Parameter	Value	Parameter	Value	Parameter	Value
$\mathbf{K_2}$	diag(0.05, 0.50, 0.75)	λ	0.25	$\mathbf{T_1}$	diag(0.75, 0.50, 1.50)
$\mathbf{K_3}$	diag(0.15, 0.40, 0.50)	Δ_u	0.65	$\mathbf{T_2}$	diag(0.75, 0.50, 1.50)
$\mathbf{K_4}$	diag(5.00, 7.50, 0.75)	Δ_p	0.05	μ_1	0.025
-	-	d_{ref}	0.05	μ_2	0.00

Observer verification

As the observer is tasked with the filtering of measurement noise, this must be verified. In Figure 9.1 an overview, and a zoomed in view of the measurements and the estimates can be seen.

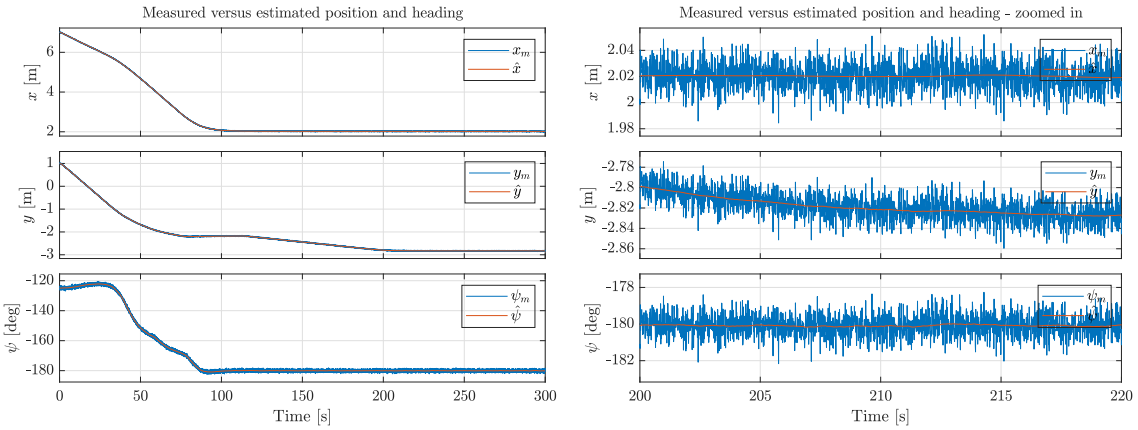

(a) Overview. (b) Zoomed in view.

Figure 9.1: Measured position and heading compared to observer estimates.

The observer is also tasked with estimating and providing signals for the unmeasured states. The provided signals for both velocity and bias can be seen in Figure 9.2.

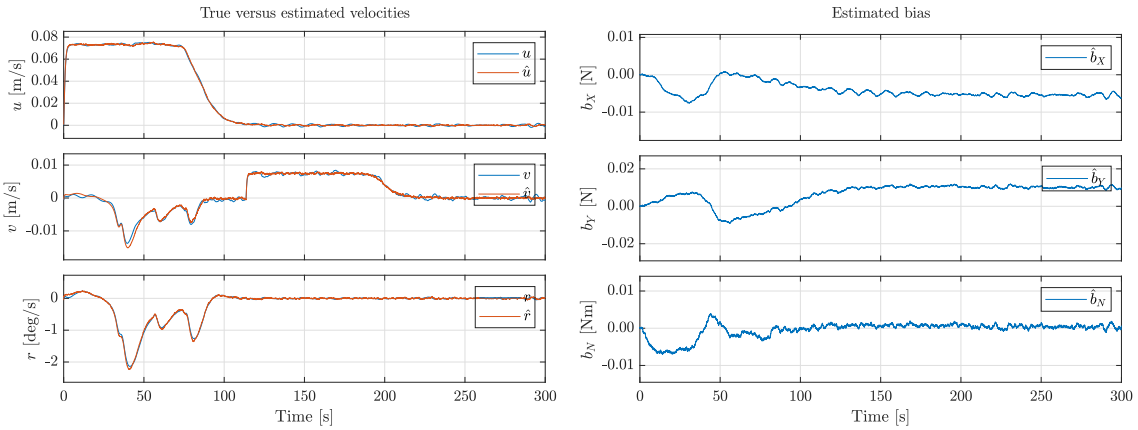

(a) Estimated body-fixed velocities. (b) Estimated bias.

Figure 9.2: Estimated velocities and bias.

From Figure 9.1b the observer can be seen to filter the measurements well, and the filtered signal seems to be around the mean of the measured signal. The provided signal for the velocities are close to the real velocities from the simulation model, and a bias signal is provided. The observer works well, providing good, feasible signals for the ADC.

9.2 Autonomous docking

In the following simulations, the ADC will be performing autonomous docking with a desired path following speed of $u_d = 0.075$ m/s and docking speed of $u_{dock} = 0.0075$ m/s. The chosen reference speeds Froude scaled to full scale corresponds to $u_d^{full} = 0.53$ m/s ≈ 1 knots, and $u_{dock}^{full} = 0.053$ m/s ≈ 0.1 knots. This docking speed is in the interval of what was found to be used in real life situations by Roubos et al. (2017). The location of the proximity sensors in the body-fixed reference frame can be seen in Table 9.2.

Table 9.2: Locations of proximity sensors in body frame.

Parameter	Value
$p_{s_1}^b$	$[0.4, 0.12]^\top$
$p_{s_2}^b$	$[-0.5, 0.12]^\top$

Five plots will be shown for each simulation of the ADC in regular operation. First a N/E plot showing the position and orientation of the ship from the observer in intervals of 30 seconds, as well as the trajectory of the ship. Second, a plot showing the measured and desired position and heading. The third plot will show the estimated body-fixed velocities plotted with the true velocities. Lastly, a plot showing the desired and yielded forces from the thrusters, and a plot showing the proximity sensor measurements will be shown.

The cases to be simulated will be as follows:

1. Regular operation.
2. Regular operation: Near-parallel entry path.
3. Regular operation: Sharp entry path.
4. Situational reactiveness: DP as response.
5. Situational reactiveness: Returning to start of Phase 2 as response.

9.2.1 Regular operation

This simulation shows the ADC in operation under normal conditions. The position and orientation of the dock is chosen to be $\boldsymbol{\eta}_{dock} = [p_{dock}^\top, \psi_{dock}]^\top = [2, -3, 0]^\top$. The start position and orientation of the vessel is set to $\boldsymbol{\eta}_0 = [7, 1, -\frac{2}{3}\pi]^\top$.

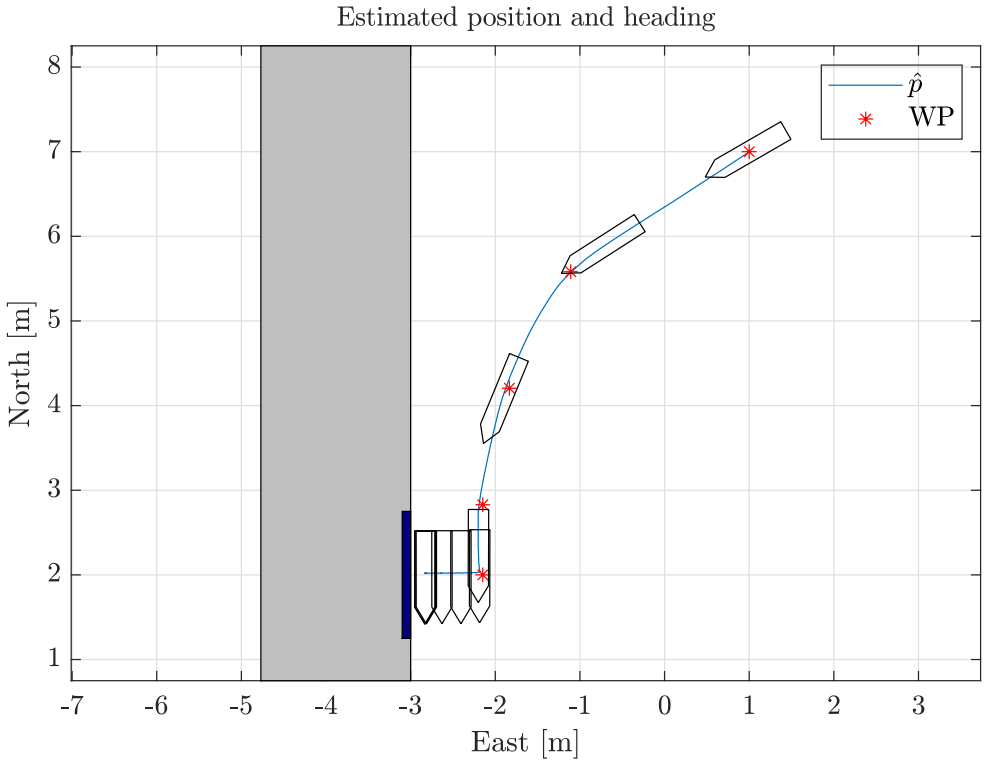

Figure 9.3: Position and heading.

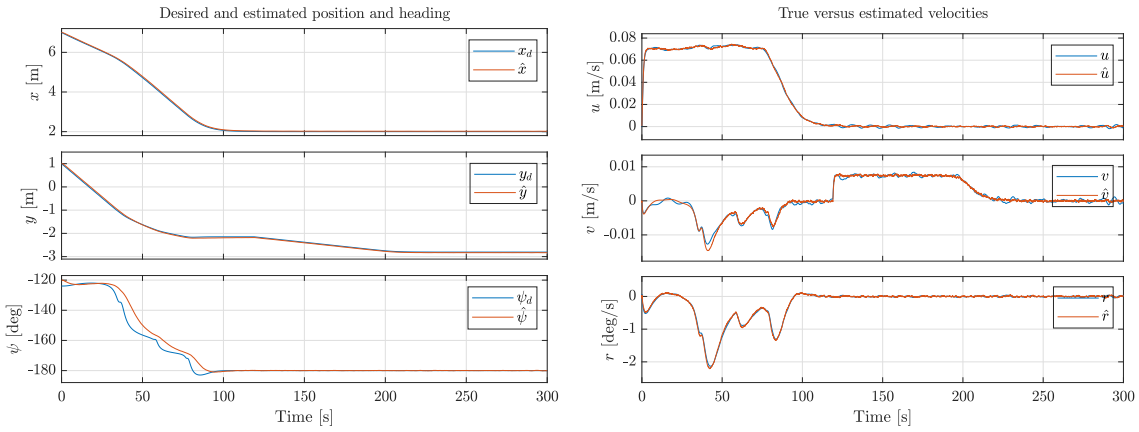

(a) Position and heading.

(b) Body-fixed velocities.

Figure 9.4: Measured and desired position and heading, and true and estimated velocities.

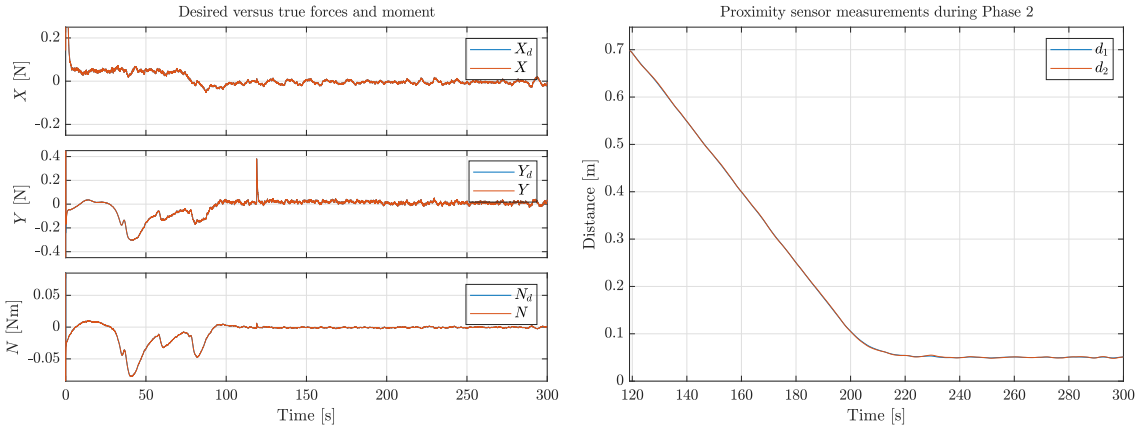

(a) Desired and yielded forces and moments.

(b) Sensor measurements during Phase 2.

Figure 9.5: Desired and yielded forces, and proximity sensor measurements.

From Figure 9.3 it can be seen that the vessel positions itself outside the designated docking location along a smooth path through the WPs, and moves at a slower pace in sway towards the dock. Figure 9.4a shows that the deviations from the desired positions in x and y are very small. The vessel seems to struggle a bit to keep up with the desired heading during Phase 1.

From Figure 9.4 it can be seen that the vessel reached the end of Phase 1 after ∼110s. Somewhere between 110-120s, the activation functions for heading correction and Phase 2 initiation is activated, starting Phase 2 at around 120s. It is apparent from Figure 9.4b that the ship is able to maintain the desired path following speed during Phase 1, and docking speed during Phase 2. In Figure 9.5a a spike can be seen in Y-direction at around 120s. This is when Phase 2 is initiated, and the vessel demands force in sway to start moving with the desired docking speed. As the thruster dynamics does not model the time it takes to build up thrust, change the direction of thrust, or spin up the propellers, the desired thrust is given almost momentarily, resulting in a spike instead of a ramp. Figure 9.5b shows that the vessel stops at the desired distance from the quayside, and remains there until the simulation is over.

9.2.2 Regular operation: Near-parallel entry path

This simulation shows the ADC in operation under normal conditions. The position and orientation of the dock is chosen to be $\boldsymbol{\eta}_{dock} = [p_{dock}^\top, \psi_{dock}]^\top = [2, -3, 0]^\top$. The start position and orientation of the vessel is set to $\boldsymbol{\eta}_0 = [7, -1.75, -\frac{17}{18}\pi]^\top$.

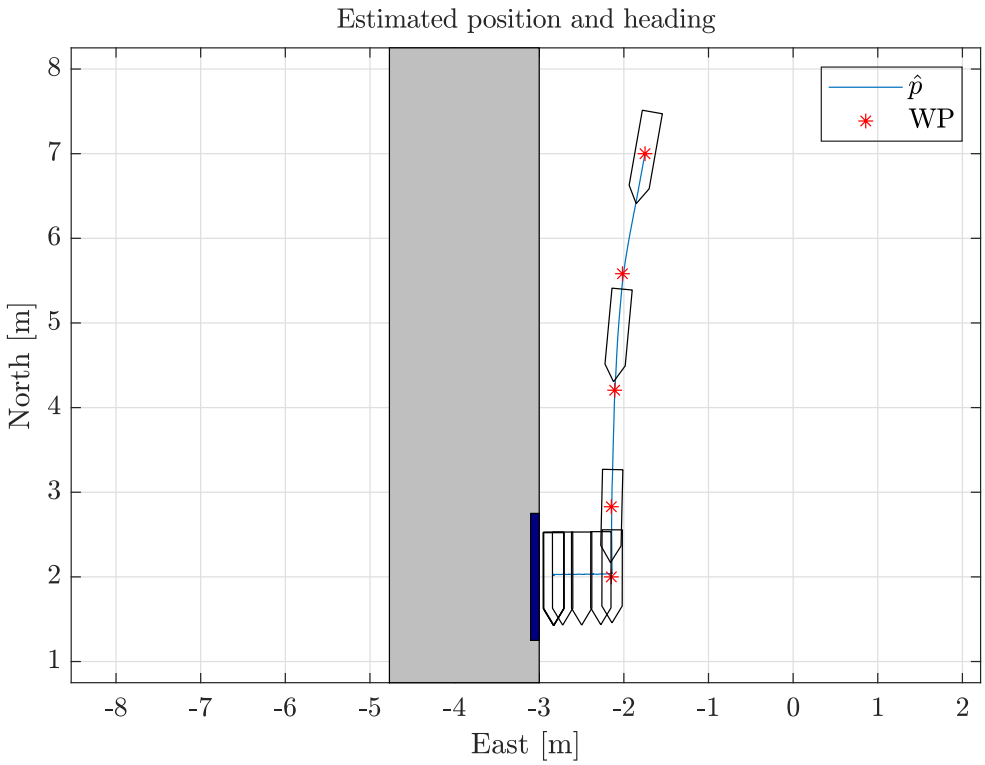

Figure 9.6: Position and heading.

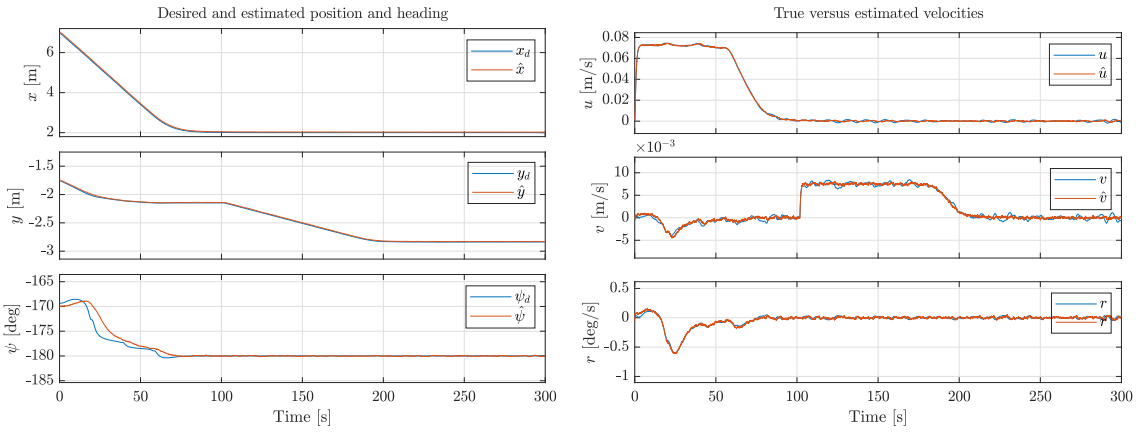

(a) Position and heading.

(b) Body-fixed velocities.

Figure 9.7: Measured and desired position and heading, and true and estimated velocities.

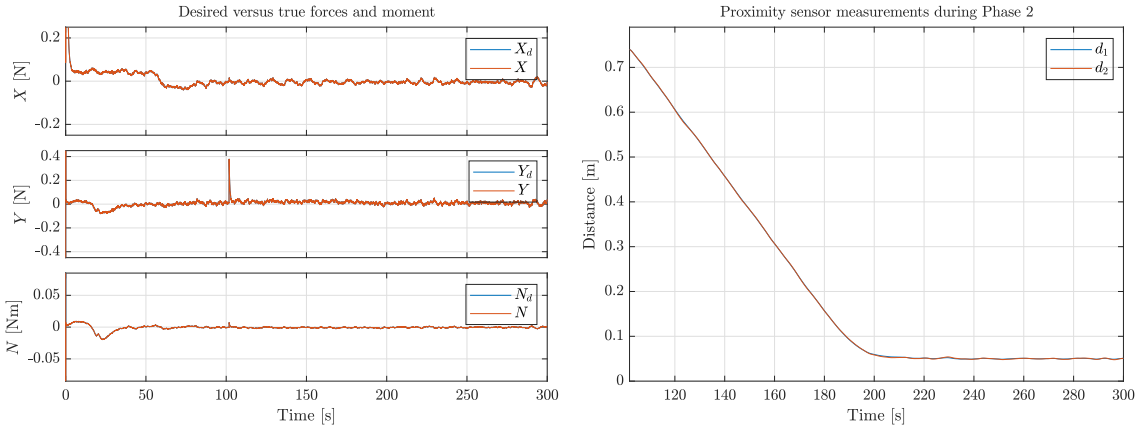

(a) Desired and yielded forces and moments.

(b) Sensor measurements during Phase 2.

Figure 9.8: Desired and yielded forces, and proximity sensor measurements.

This simulation yields very similar results to the previous. From Figure 9.6 and Figure 9.7a it can be seen that the vessel performs slightly better when approaching the second to last waypoint, and on the last path segment, before arriving at the end of Phase 1. This is likely due to the lower demand in heading change along the desired path, which again leads to better path following. Phase 1 ends at about 100s, and Phase 2 is started shortly after, as can be seen in Figure 9.7b as the vessel starts moving in sway. The vessel is able to maintain the desired speeds in each phase of the operation, and Figure 9.8a shows lower demand in heading change. Figure 9.8b shows that the vessel stops at the desired reference distance.

9.2.3 Regular operation: Sharp entry path

This simulation shows the ADC in operation under normal conditions. The position and orientation of the dock is chosen to be $\boldsymbol{\eta}_{dock} = [p_{dock}^\top, \psi_{dock}]^\top = [2, -3, 0]^\top$. The start position and orientation of the vessel is set to $\boldsymbol{\eta}_0 = [6, 4, -\frac{7}{12}\pi]^\top$.

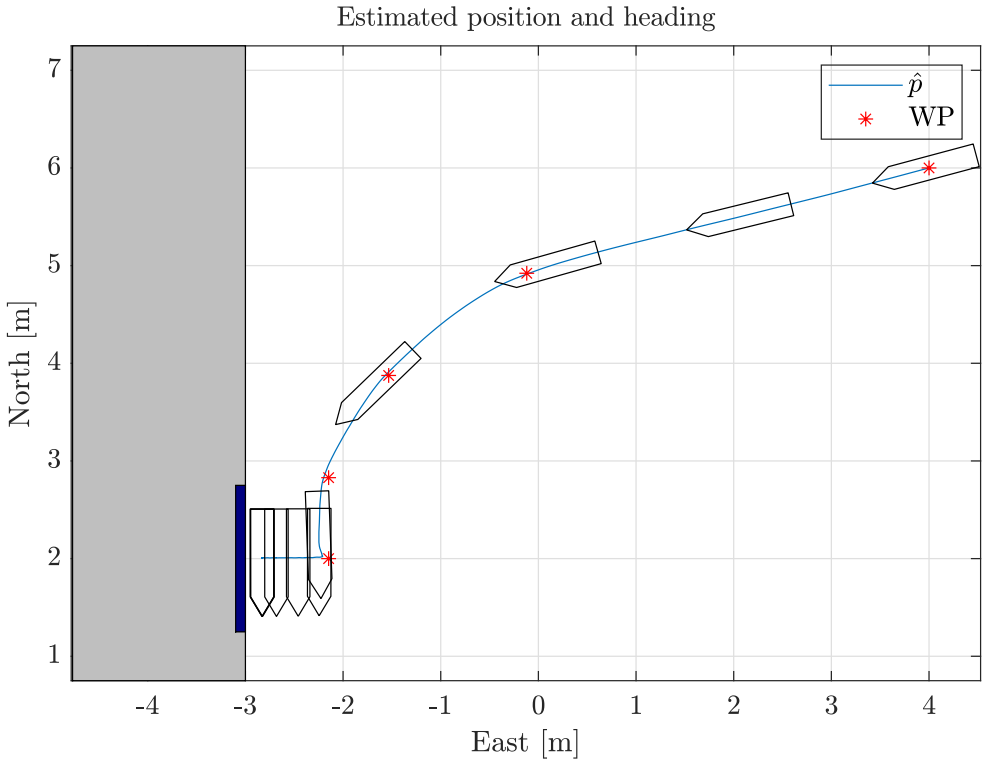

Figure 9.9: Position and heading.

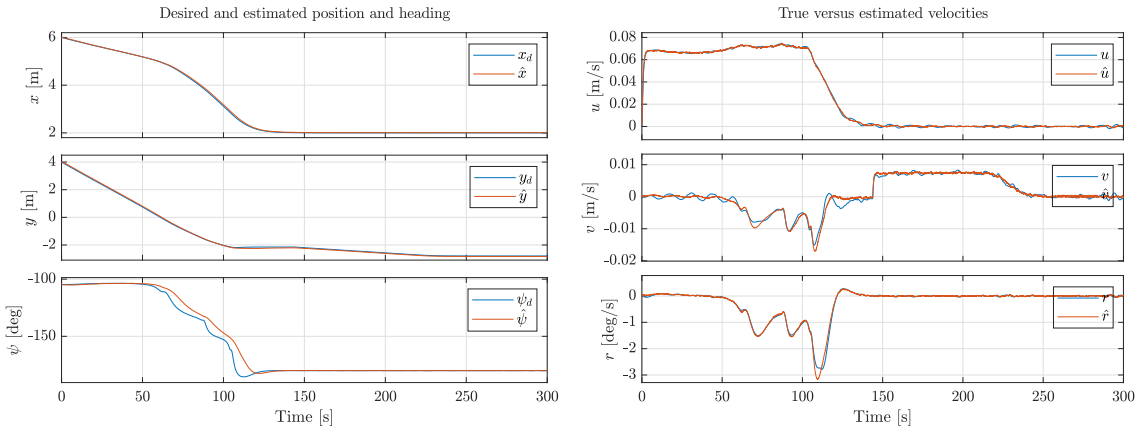

(a) Position and heading.

(b) Body-fixed velocities.

Figure 9.10: Measured and desired position and heading, and true and estimated velocities.

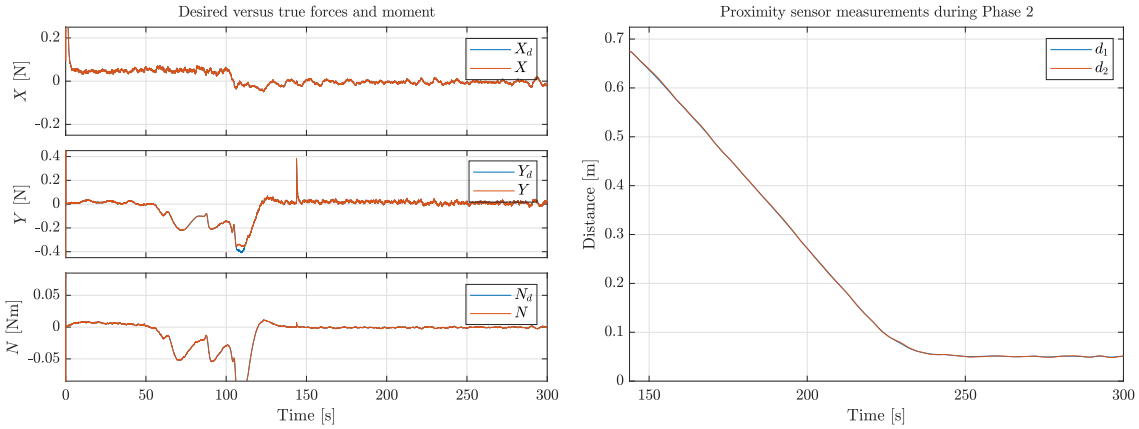

(a) Desired and yielded forces and moments.

(b) Sensor measurements during Phase 2.

Figure 9.11: Yielded and desired forces, and proximity sensor measurements.

Similar results as the two previous simulations are achieved. In this simulation the vessel struggles more when closing in on the second to last WP, and on the last path segment, as shown in Figure 9.9. This is most likely due to the high demand in heading change caused by the initial position resulting in a sharp entry path, as can be seen in Figure 9.10a and Figure 9.11a. The vessel struggles to keep the desired heading throughout Phase 1. Phase 2 is initiated at around 140s, and is completed satisfactorily, both with respect to the desired docking speed, and the reference distance, as seen in respectively Figure 9.10b and Figure 9.11b.

9.2.4 Situational reactiveness: Obstacle entering docking path

The following simulations are meant to demonstrate the situational reactiveness discussed in Section 6.3.4. The first method for drop detection is used, checking the previous measurement versus the current. Both discussed reactions will be demonstrated, the first one being enabling DP at the current position ($u_{dock} = 0$), and the second one being to return to the start of Phase 2 as presented in Equation 6.22. The threshold for detected danger, ϵ_1, is set to 0.01 m which is equal to 0.5 m in full scale.

The obstacle will result in a drop of 0.1 m in the measurement, 5 m in full scale, and be introduced to proximity sensor 1 after 150s, when the vessel is around half way through Phase 2. After 100s, at 250s, the obstacle is removed. The total simulation time is 400s.

These simulations are also included as animations in Appendix B, which may give a better understanding and overview of the operation.

Enabling DP as response to danger

To illustrate the reaction to danger, the vessel will be plotted in red as long as danger is detected.

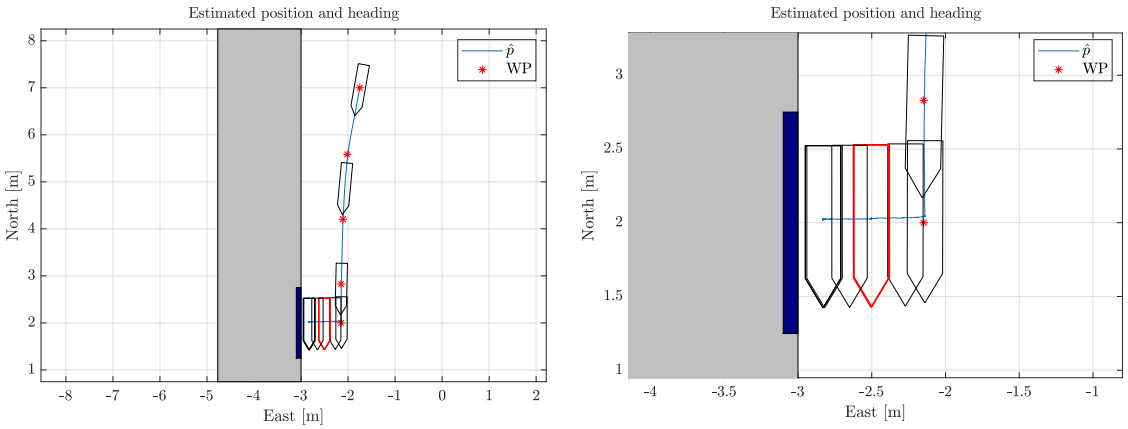

(a) Overview.

(b) Zoomed in view during Phase 2.

Figure 9.12: Position and heading during the operation.

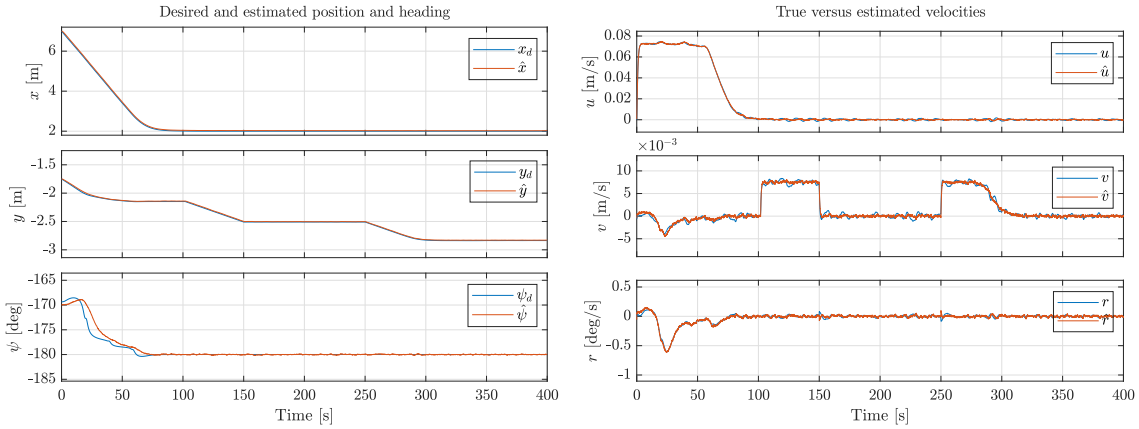

(a) Position and heading. (b) Body-fixed velocities.

Figure 9.13: Measured and desired position and heading, and true and estimated velocities.

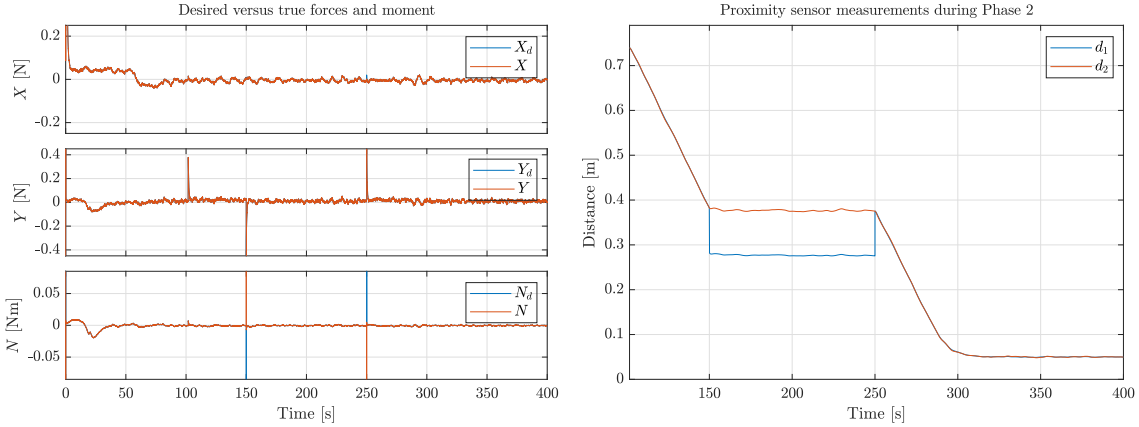

(a) Desired and yielded forces and moments. (b) Sensor measurements during Phase 2.

Figure 9.14: Yielded and desired forces, and proximity sensor measurements.

As the the near-parallel entry case is used, the performance up until the obstacle appears are identical to that discussed in Section 9.2.2. After 150s, a drop in the measurement of sensor 1 can be seen in Figure 9.14b. In Figure 9.13b it can be seen that the velocity in sway goes down to zero, and Figure 9.13a shows that the vessel remains in place up until 250s. This 100 second interval of DP operation can be seen in Figure 9.12, with the vessel plotted in red. When the detection of a jump in the measurement corresponding to the original drop is detected after 250s, the vessel starts moving in sway again. The operation ends just after 300s, with the ship stopping at the desired reference distance and remaining there until the simluation is over.

Returning to start of Phase 2 as response to danger

As it is difficult to illustrate the vessel moving back and forth in the same direction in the same N/E-plot, the operation will be split up in three different N/E-plots. The first will show the operation from start to danger detection, the second will show the operation during danger detection, and the last will show from the danger is gone and to the end of the operation. The vessel will be plotted in red while danger is detected.

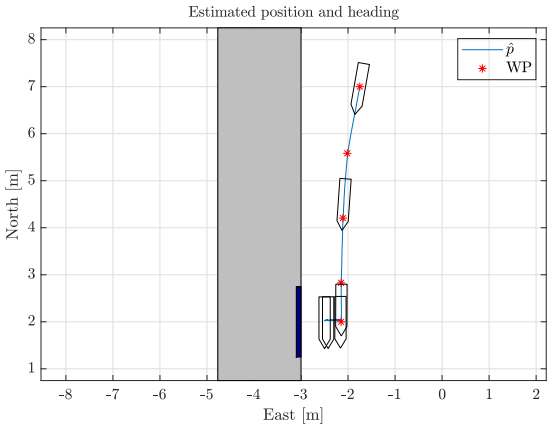

(a) Operation before danger (0-150s).

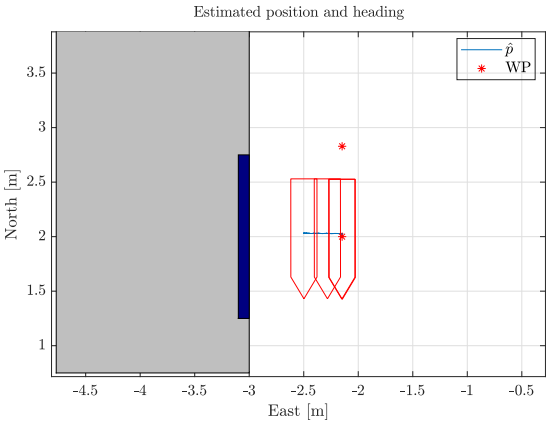

(b) Operation during danger (150-250s).

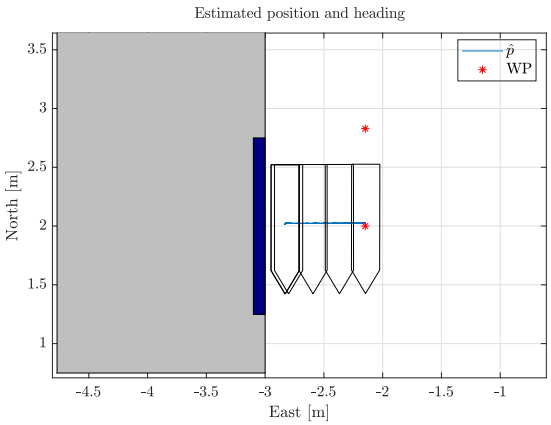

(c) Operation after danger (250-400s).

Figure 9.15: Position and heading during operation.

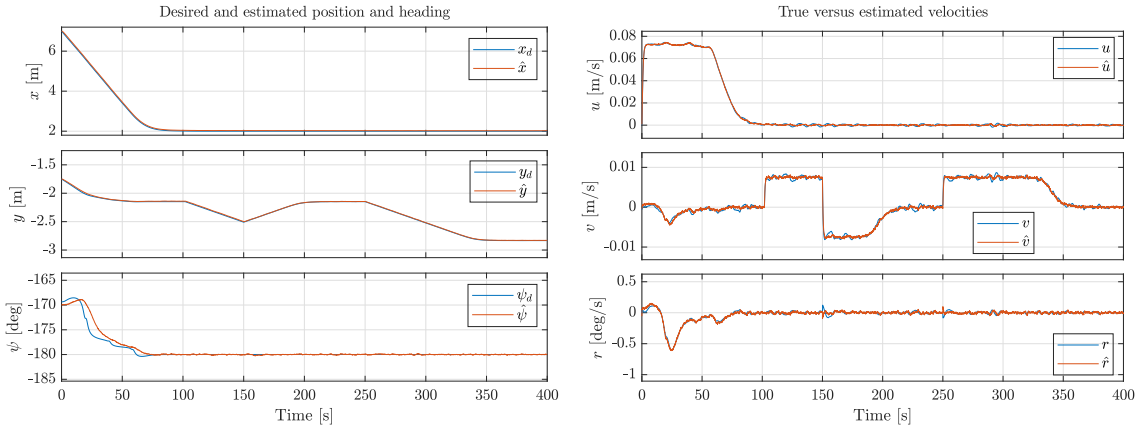

(a) Position and heading. (b) Body-fixed velocities.

Figure 9.16: Measured and desired position and heading, and true and estimated velocities.

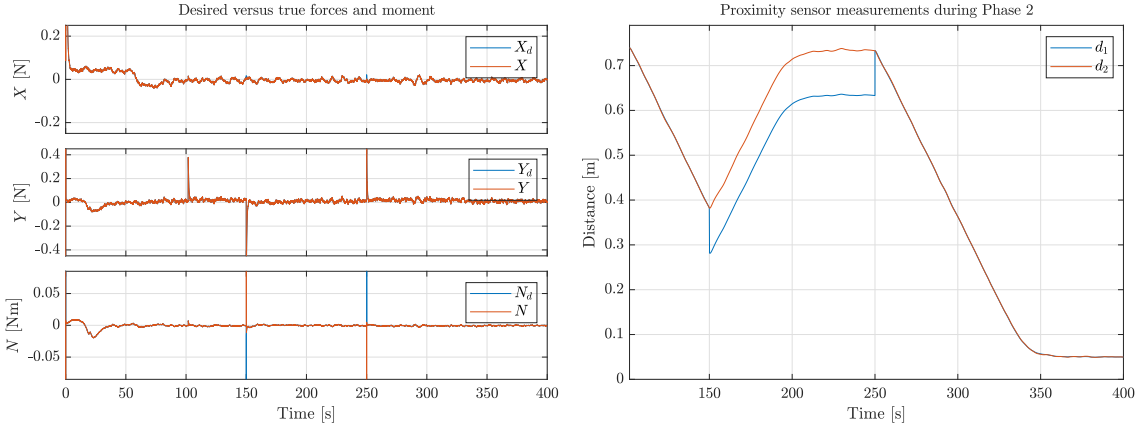

(a) Desired and yielded forces and moments. (b) Sensor measurements during Phase 2.

Figure 9.17: Desired and yielded forces and moment, and proximity sensor measurements.

The situation leading up to obstacle detection is the same as in the previous simulation. During this simulation the vessel is to move back to the start of Phase 2 when detecting danger. As can be seen in Figure 9.16b the vessel changes direction of the sway motion when the obstacle is introduced at 150s, and gradually comes to rest at the location of Phase 2 initiation, as seen in Figure 9.16a. The proximity sensor readings in Figure 9.17b illustrates the same behavior, going back to, and staying at the initial measurement at the start of Phase 2. The whole operation is illustrated in Figure 9.15, with Figure 9.15b showing the ship moving from approximately -2.5 m, and back out to around -2.15 m in east direction.

9.3 Discussion

The operation is undertaken in a satisfying way for all simulations. The path following phase shows good tracking, except for some deviations which become larger when there is demand for larger heading change over short time or distance. The guidance laws generate a docking path, and control the speed of the vessel well, with the vessel slowing down and coming to a rest when nearing the end point of each phase. For the situational reactiveness, the vessel reacts as expected to the detected danger, and completes the docking in a similar manner as before when the obstacle is removed.

To ease the vessel from the demanded heading changes, a different path planning could be considered. The path planning used in this thesis is strict and fixed for each scenario. Different path planning algorithms could also be used for different initial positions and entry paths. Also, as different vessels have different actuators, available power, and actuation, the path planner could take vessel specific properties and characteristics into account to provide a more optimal path planning.

The employed path planner places a WP a set distance behind the last WP, ensuring a near dock-parallel entry to the last WP. This is done to make the docking path, which goes along the normal vector of the last path segment, to be perpendicular to the dock. As the heading is set to be path tangential in Phase 1, the vessel will already have, in theory, a near parallel heading to the dock when engaging the heading correction. This leads to the calculated heading correction being very small. In Appendix A a simulation of the first case is run, removing the second to last WP. The same simulation can be found animated in Appendix B. In that simulation it can easily be seen that the vessel arrives at the last WP not aligned with the dock, and the heading correction is clearly visible in the plot over desired heading, as a jump. A reference model could be added to avoid the heading correction as a jump. The ship still undertakes the operation in a satisfying manner, but the effect of the docking path not coming in perpendicular to the dock can be seen clearly. This might not be desirable, for example if the assigned docking spot has a tight clearance. A solution to this could be to skew the normal vector by using the heading correction calculation, this way one could remove the second to last WP while still ensuring a docking path perpendicular to the quayside.

Another factor that affects the performance of the vessel and the operation, is the tuning of the motion controller. The tuning process of the uncoupled cascaded backstepping controller proved to be challenging, and hard to understand. From the plots of the desired and yielded forces and moments it can be seen that the signals are a little noisy. During the tuning process it was found that the tuning parameters heavily affected both this noise, and the ability of the vessel to perform path following. It was easier to find gains yielding good results when violating $\mathbf{T_2} < \mathbf{T_1}$, and much time was spent on finding gains that provided good results while still satisfying this constraint.

The situational awareness and reactiveness implemented by the use of the proximity sensors are simple, but rather effective. The downside is that the vessel does not know what is going on in the environment around itself. There are no object tracking, object recognition, or environmental scanning, just a distance measurement. It can be debated if a system just based on distance measurements even qualifies to be called a situational awareness system as a stand-alone component. With that being said, it may prove useful as an add-on to other sensors and components making up a situational awareness system. By combining other sensors providing other information, a more educated and informed desired reaction could be chosen depending on the provided overview of the situation. Coming to a complete stop, or returning to the start of Phase 2 could be good candidates for reactions to turn to, and the ADC performed these reactions in a good way. In this thesis the danger was considered removed when a jump equal to the detected drop was detected. The method for considering it safe to start the docking process again should be more sophisticated, maybe utilizing a situational awareness system that takes more information about the surroundings into account, or even human confirmation.

The plots of the desired and yielded forces and moment show some spikes, especially in the transition between phases, and during velocity direction changes. The yielded forces would in reality not be able to behave in such a way, due to physical limitations of the thrusters. Limits to how fast the thrust direction can be changed, how fast the spin of the propeller can be changed, and thruster loss due to the speed of the ship are not modeled in the simulations. The max thrust available from each thruster was measured in the laboratory with unknown accuracy and precision. There is reason to suspect that the measurements taken of the thrusters might be inaccurate because the forces from the thrusters on the model ship are quite small and the measurement noise on the measurement devices used were quite high.

Lastly, the measurements from the proximity sensors would in a real-world scenario be clouded with measurement noise. This would have to be filtered out in the observer. As for the simulations done in this thesis, measurement noise has not been added to the proximity sensor modeling, and the proximity sensors signal is just sent straight through the observer. If measurement noise was to be modeled for the proximity sensors, it could have been done in a similar manner of what was done to the position and orientation measurements, by adding zero-mean Gaussian white noise.

Chapter 10

Conclusions and further work

10.1 Conclusions

This thesis has designed an autonomous docking controller aiming to utilize a conventional sensor suite aided by simple proximity sensors. The ADC has been tested and verified in simulation studies with good results. A solution to add situational awareness to the system by using the proximity sensor measurements has been explored, as well as appropriate reactions when danger is detected. Tests were also run on the situational reactiveness, with satisfying results.

The path planning algorithm worked well in most scenarios, but is very strict and rigid for all initial positions of the vessel. The chosen path planning algorithm is not considered the most optimal choice, and other solutions could be better despite the chosen one yielding good results.

The guidance system worked well, performing path following for Phase 1, and generating a docking path and following this with an appropriate heading during Phase 2. The desired reference speed during each phase was maintained, and the vessel came to a halt at the end of both phases at the desired position. The proximity sensors were used to provide a heading correction before initiating Phase 2, as well as dictating the speed along the docking path.

The situational awareness implemented was simple but effective. It is questioned if it is sufficient to be used a stand alone system, but it could prove useful as a compliment to a larger, more complex situational awareness system. The reactions used and tested when detecting danger was to stop the vessel and enable DP, and to stop the vessel and move back to the start of the docking phase. These reactions were viewed as good, appropriate candidates for reactions in a docking scenario, and the ADC performed these actions well.

10.2 Further work

In this section recommendations for further work regarding safe autonomous docking will be presented.

One of the main areas for further development and work would be regarding the path planning. The maneuvering preceding the docking operation in Phase 2 should be researched to find more optimal solutions. As mentioned earlier, the path planner could take into account the vessel position and orientation with respect to the dock, as well as the vessel and thruster characteristics when planning the path. A path planner could also take other constraints into account, such as time, energy consumption, and ship traffic. It could also be interesting to look into developing a global path planner applicable for the voyage as a whole, including maneuvering out from a harbor, transit, harbor entrance and maneuvering, and docking.

Another area of importance in regards to a safe and effective docking operation is the situational awareness and reactiveness system. Effort should be put into developing a robust and reliable situational awareness system providing in-depth information of the vessel surroundings. This system may, or may not, be using proximity sensors. Also, a decision making system getting information from the situational awareness system could be made to determine the best or optimal reaction to different situations a vessel might encounter during operation. Reactions to resort to should be further researched and explored, the more alternatives of action a system are to chose from, the greater are the probability of a satisfying and optimal reaction to each situation. Reactions could for example incorporate rules from the Convention on the International Regulations for Preventing Collisions at Sea by the International Maritime Organization, as well as simpler maneuvers of the like of the ones explored in this thesis.

As access to the laboratories was denied while this thesis was being written, it is suggested and recommended to experimentally verify the ADC.

Bibliography

Allianz (2017). *Ready to launch: Autonomous Ships - Smart Sails.*
URL: *https://www.allianz.com/en/press/news/business/insurance/170824-autonomous-shipping-smart-sails.html (**Accessed:** 03.02.2020)*

Dubins, L. E. (1957). On curves of minimal length with a constraint on average curvature and with prescribed initial and terminal positions and tangents, *American Journal of Mathematics* **79**(3): pp. 497–516. doi: 10.2307/2372560.

Fossen, T. I. (2000). Nonlinear Passive Control and Observer Design for Ships, *Journal of Modeling, Identification and Control* **21**(3): pp. 129–184. doi: 10.4173/mic.2000.3.1.

Fossen, T. I. (2011). *Handbook of Marine Craft Hydrodynamics and Motion Control*, West Sussex: John Wiley & Sons, Ltd.

Gauslaa, E. (2019). *Navigation, guidance, and control for autonomous autodocking of ships*, Project Thesis, Trondheim.

Kongsberg (n.d.a). *LASER-BASED POSITION REFERENCE SYSTEM.*
URL: *https://www.kongsberg.com/maritime/products/vessel-reference-systems/position-systems/laser-based-position-reference-system (**Accessed:** 03.02.2020)*

Kongsberg (n.d.b). *RELATIVE POSITION REFERENCE SYSTEM, RADIUS.*
URL: *https://www.kongsberg.com/maritime/products/vessel-reference-systems/position-systems/relative-position-reference-system-radius/#technicalInformation (**Accessed:** 02.03.2020)*

Kálmán, R. E. (1960). A New Approach to Linear Filtering and Prediction Problems, *Journal of Basic Engineering* **82**(1): pp. 35–45. doi: 10.1115/1.3662552.

Lekkas, A. M. (2014). *Guidance and Path-Planning Systems for Autonomous Vehicles*, PhD thesis, NTNU, Trondheim.

Minorsky, N. (1922). DIRECTIONAL STABILITY OF AUTOMATICALLY STEERED BODIES, *Journal of the American Society for Naval Engineers* **34**: pp. 280–309. doi: 10.1111/j.1559–3584.1922.tb04958.x.

Murdoch, E., Dand, I. W. and Clarke, C. (2012). *A Master's Guide to Berthing*, 2nd edn, London: Standard House.

NTNU (2020). *CyberShip Enterprise I - User Manual*, Trondheim: Department of Marine Technology.

Roubos, A., Groenewegen, L. and Peters, D. J. (2017). Berthing velocity of large seagoing vessels in the port of Rotterdam, *Marine Structures* **51**: pp. 202–219. doi: 10.1016/j.marstruc.2016.10.011.

Skjetne, R. (2005). *The Maneuvering Problem*, PhD thesis, NTNU Department of Engineering Cybernetics, Trondheim, Norway.

Skjetne, R. (2019a). Lecture 8: DP Control System, *TMR4243: Marine Control Systems II* .
URL: *https://ntnu.blackboard.com* (***Accessed:*** *08.04.2020)*

Skjetne, R. (2019b). Notes on: Guidance and maneuvering design for docking - Revision A.

Skjetne, R. (2020). Technical note: Maneuvering-based guidance design for dynamic positioning - Revision B.

Sørensen, A. J. (2018). *Marine Cybernetics, Towards Autonomous Marine Operations and Systems*, Lecture Notes UK-18-73, Department of Marine Technology, NTNU, Trondheim.
URL: *http://folk.ntnu.no/assor/Public/2018-08-20%20marcyb.pdf* (***Accessed:*** *12.02.2020)*

Wärtsilä (n.d.). *Artemis*.
URL: *https://www.wartsila.com/marine/build/dynamic-positioning/artemis* (***Accessed:*** *03.02.2020)*

Appendix A

Removing second to last WP

The following plots are from a simulation with the inital conditions from subsection 9.2.1, but removing the second to last WP. This simulation is included to illustrate the applied heading correction and the docking path not being perpendicular to the dock in this case.

An animation of this simulation can be found in Appendix B.

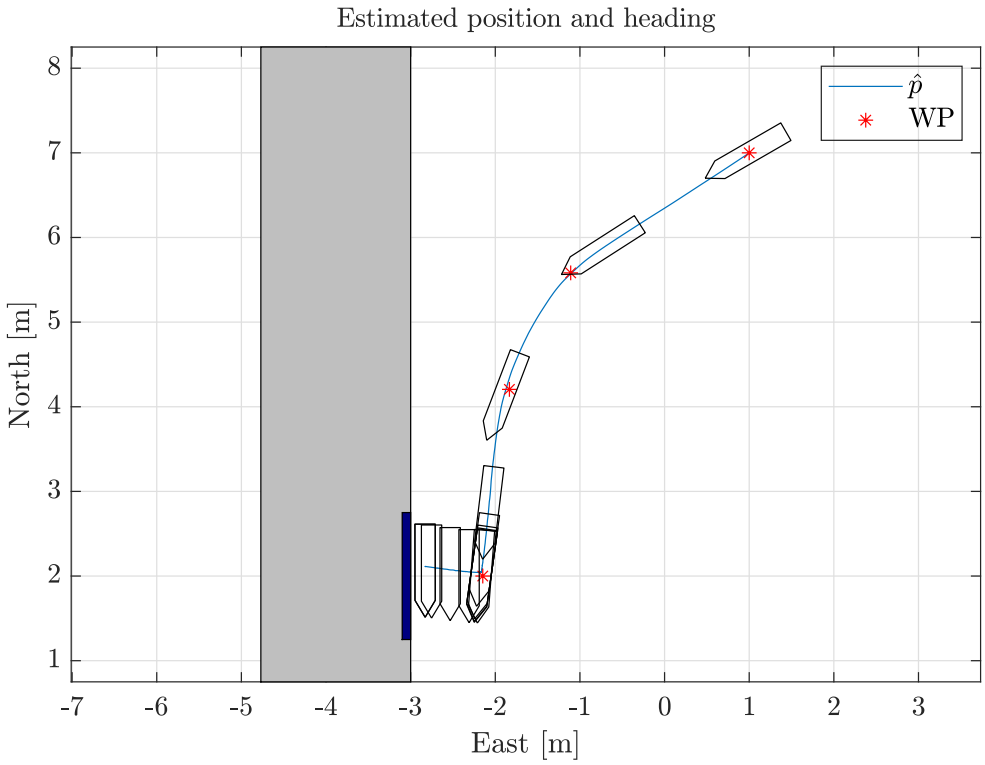

Figure A.1: Position and heading.

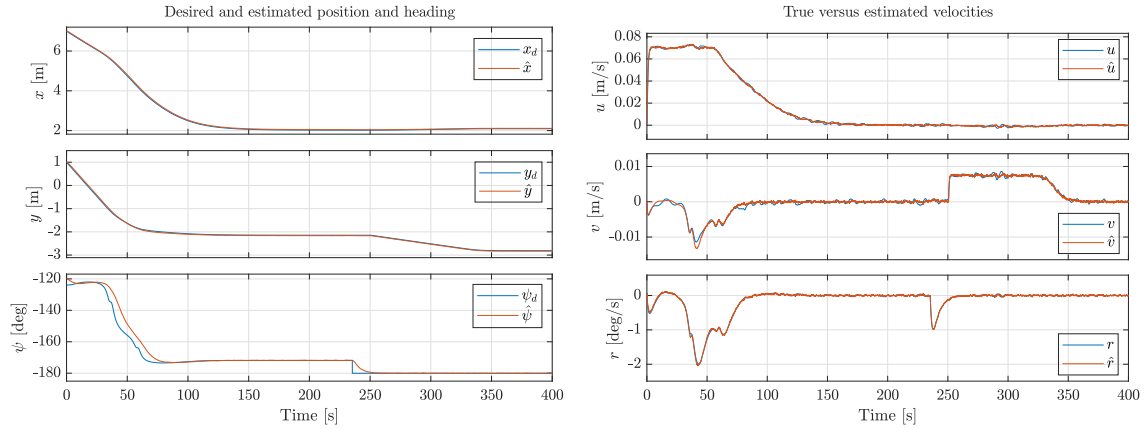

(a) Position and heading. (b) Body-fixed velocities.

Figure A.2: Measured and desired position and heading, and true and estimated velocities.

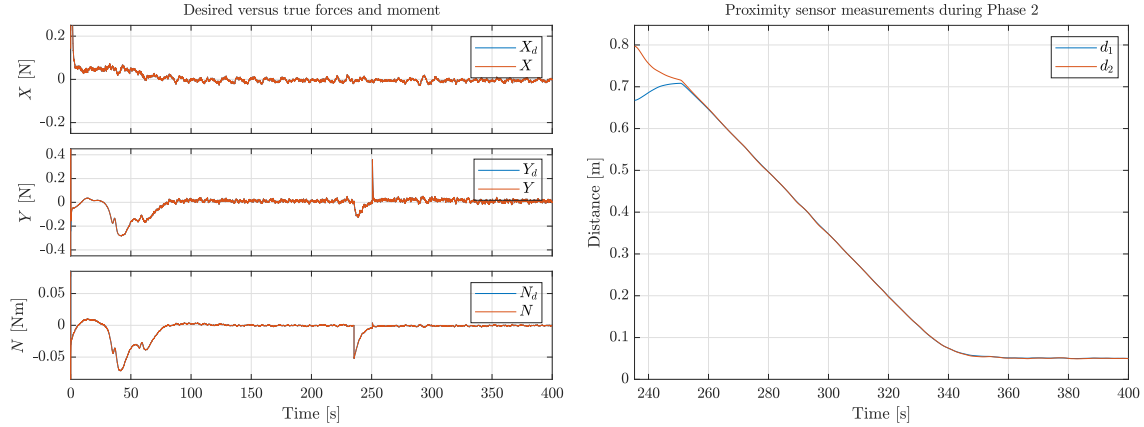

(a) Desired and yielded forces and moments. (b) Sensor measurements during Phase 2.

Figure A.3: Yielded and desired forces, and proximity sensor measurements.

Appendix B

Animations of simulations

https://vimeo.com/426191224

(a) 1. Regular operation.

https://vimeo.com/426191246

(b) 2. Regular operation: near-parallel.

Figure B.1: QR-codes to animations.

https://vimeo.com/426191268

(a) 3. Regular operation: sharp entry.

https://vimeo.com/426191291

(b) 4. Situational reactiveness: DP.

Figure B.2: QR-codes to animations.

https://vimeo.com/426191309

(a) 5. Situational reactiveness: Return.

https://vimeo.com/425872461

(b) Appendix A animation: Removed p_3.

Figure B.3: QR-codes to animations.

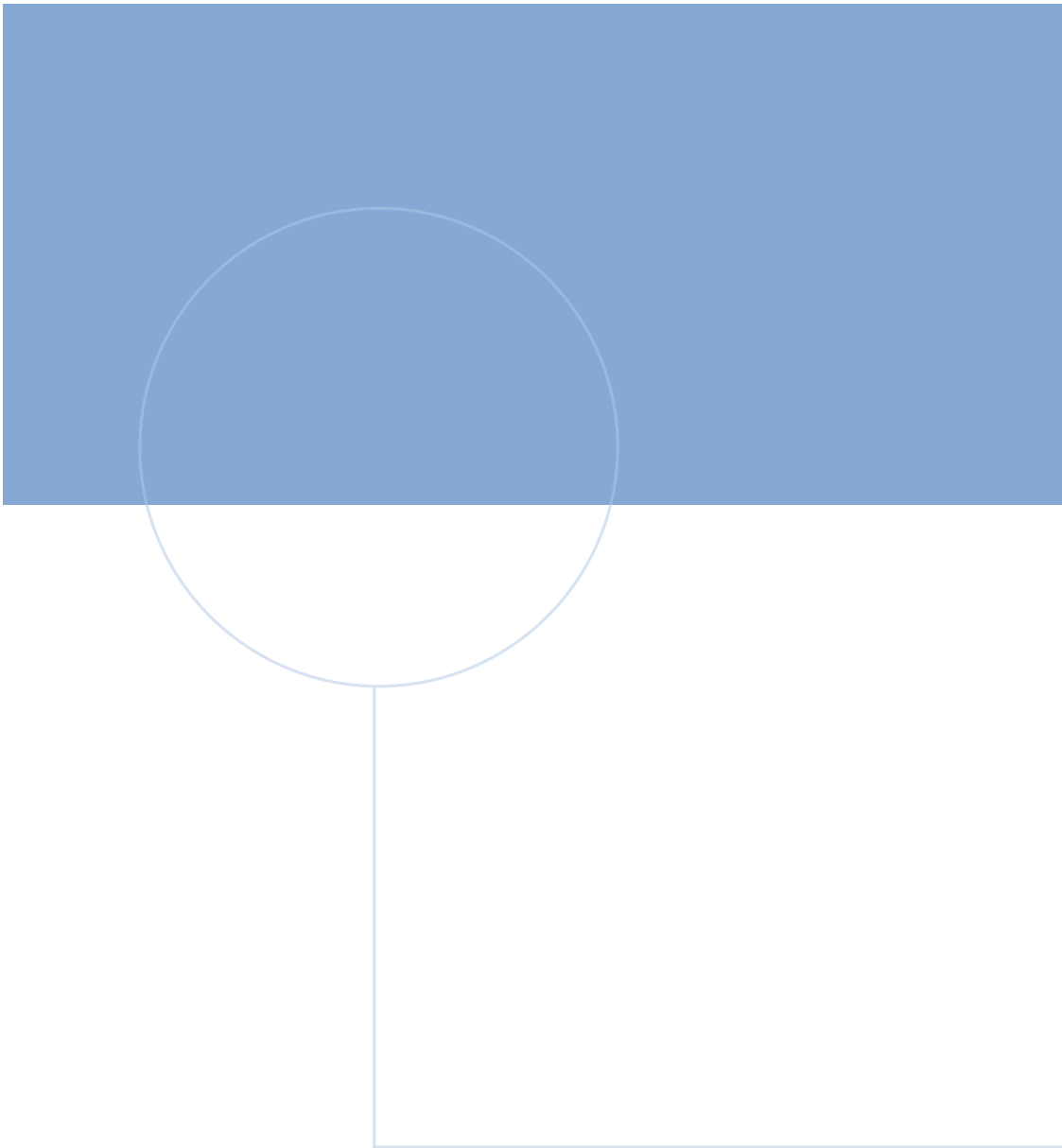

NTNU

Norwegian University of
Science and Technology